

# A Search for Multi-Planet Systems Using the Hobby-Eberly Telescope<sup>1</sup>

Robert A. Wittenmyer<sup>2,3</sup>, Michael Endl<sup>2</sup>, William D. Cochran<sup>2</sup>, Harold F. Levison<sup>4</sup>,  
Gregory W. Henry<sup>5</sup>

rob@phys.unsw.edu.au

## ABSTRACT

Extrasolar multiple-planet systems provide valuable opportunities for testing theories of planet formation and evolution. The architectures of the known multiple-planet systems demonstrate a fascinating level of diversity, which motivates the search for additional examples of such systems in order to better constrain their formation and dynamical histories. Here we describe a comprehensive investigation of 22 planetary systems in an effort to answer three questions: 1) Are there additional planets? 2) Where could additional planets reside in stable orbits? and 3) What limits can these observations place on such objects? We find no evidence for additional bodies in any of these systems; indeed, these new data do not support three previously announced planets (HD 20367b: Udry et al. 2003, HD 74156d: Bean et al. 2008, and 47 UMa c: Fischer et al. 2002). The dynamical simulations show that nearly all of the 22 systems have large regions in which additional planets could exist in stable orbits. The detection-limit computations indicate that this study is sensitive to close-in Neptune-mass planets for most of the systems targeted. We conclude with a discussion on the implications of these non-detections.

*Subject headings:* stars: planetary systems – extrasolar planets

---

<sup>1</sup>Based on observations obtained with the Hobby-Eberly Telescope, which is a joint project of the University of Texas at Austin, the Pennsylvania State University, Stanford University, Ludwig-Maximilians-Universität München, and Georg-August-Universität Göttingen.

<sup>2</sup>McDonald Observatory, University of Texas at Austin, Austin, TX 78712

<sup>3</sup>Department of Astrophysics, School of Physics, University of NSW, 2052, Australia

<sup>4</sup>Department of Space Studies, Southwest Research Institute, Boulder, CO 80302

<sup>5</sup>Center of Excellence in Information Systems, Tennessee State University, 3500 John A. Merritt Blvd., Box 9501, Nashville, TN 37209, USA

## 1. Introduction

About 12% ( $N = 31$ ) of known planetary systems contain more than one planet. Now that radial-velocity precision at the  $1\text{-}2 \text{ m s}^{-1}$  level is being achieved by several planet search programs (Butler et al. 2006; Lovis et al. 2006), Neptune-mass planets are becoming detectable. Recent discoveries of “super-Earths” ( $m \sin i \lesssim 10 M_{\oplus}$ ) by the High-Accuracy Radial Velocity Planet Search (HARPS) instrument (Bouchy et al. 2008; Mayor et al. 2009; Udry et al. 2007; Bonfils et al. 2007) suggest that super-Earths may be common.

The presence of close-in giant planets (“hot Jupiters”) inferred by precision radial-velocity surveys has emphasized the importance of post-formational dynamical evolution processes such as planetary migration. The core-accretion model of planetary formation (Lissauer 1995; Pollack et al. 1996) posits that rocky cores form in the outer regions of the protoplanetary disk and experience runaway gas accretion once they reach a mass of  $\sim 10$  Earth masses. These giant planets then migrate inward to become hot Jupiters (Bodenheimer et al. 2000). Alternatively, the disk-instability model suggests that such planets form by direct gravitational collapse of the protoplanetary disk (Boss 1995, 1998). Multi-planet systems can be formed by this method (Boss 2003), though subsequent evolution can easily eject planets, resulting in a wide variety of system end-states (Levison et al. 1998). The discovery of additional multi-planet systems will provide valuable added constraints to these two models of planet formation. Trilling et al. (1998) have proposed that gas giant planets migrating inward can overflow their Roche lobes and be stripped of their gaseous envelopes. Under the core-accretion model of planet formation, a Neptune-mass rocky core would then remain in a close orbit, and the detection of such objects would lend support to that theory. Alternatively, the nondetection of close-in, low-mass ( $m_p < 15 M_{\oplus}$ ) planets would tend to favor the disk-instability model, in which gas giant planets have no solid cores. Hence, an intensive effort to characterize the population of detectable planets around nearby stars will be extremely valuable for understanding the processes of planet formation and evolution.

The architectures of multi-planet systems can shed light on their formation and dynamical history. Chatterjee et al. (2008) performed simulations of systems with three giant planets and found that at least one planet would be ejected before the system stabilised. When two planets remained (80% of cases), their median eccentricities were  $e \sim 0.4$ . Similarly, randomly generated planetary systems simulated by Jurić & Tremaine (2008) typically retained 2-3 giant planets after  $10^8$  yr. That all five planets (Fischer et al. 2008) in the 55 Cancri system have relatively low eccentricities ( $e < 0.2$ ) suggests that systems with inactive dynamical histories (i.e. free of major perturbation events) may be able to retain several giant planets in nearly circular orbits.

The final configuration of a planetary system is dependent on the post-formation migration and dynamical interaction processes. Mandell et al. (2007) showed that the migration of a Jupiter-mass planet through a disk of planetesimals can result in the formation of an interior terrestrial-mass planet. Simulations of known multi-planet systems by Barnes & Quinn (2004) and Barnes & Raymond (2004) suggest that planetary systems are “packed” – that is, they contain the maximum number of planets that is dynamically possible. Barnes & Raymond (2004) investigated the dynamically stable regions of the HD 74156 system. Those authors used the results to predict that an additional planet, between planets b and c, could be present. The detection by Bean et al. (2008) of such an object lends support to the “packed planetary systems” hypothesis (Barnes et al. 2008), which would imply that multiple-planet systems are common. However, our own results (see § 3) do not support this hypothesis.

A series of papers by Ida & Lin (Ida & Lin 2004a,b) predicts a paucity of planets of 10-100 Earth masses within  $\sim 1$  AU (the “planet desert”). Their core-accretion simulations also predict an abundance of close-in ( $a \lesssim 0.1$  AU) planets with masses below about  $10 M_{\oplus}$ . Ida and Lin further suggest that the distribution of planetary mass vs. semimajor axis will constrain the dominant formation processes of planets. In a subsequent paper, Ida & Lin (2008) show that the frequency of giant planets depends sensitively on the Type I migration rate, which must be slowed by a factor  $C_1 \sim 0.03-0.1$  in order to reproduce the distribution of detected planets.

In this work, we describe an intensive three-year radial-velocity campaign to search for additional planets in known planetary systems (§ 2). Section 3 gives the results of the orbit fits and the search for new planets, with discussion about a few of the interesting systems. Section 4 describes the dynamical simulations used to determine the regions in each system where additional planets could reside in stable orbits. The detection limits, which determine the sensitivity of this survey, are presented in § 5. Finally, Section 6 assesses the impact of these new data and analyses on the theories of planet formation and the population-level statistics of extrasolar planets. This work thus presents a three-fold approach to the question of planetary system architecture: 1) Are additional planets present in these known planetary systems? 2) Where could additional objects reside in stable orbits? 3) What limits can be placed on such objects?

## 2. Observational Data

Twenty-two targets were chosen for this project from the list of  $\sim 150$  planet hosts known in 2004 September. A majority of the observational data were obtained at McDonald Ob-

servatory with the 9.2 m Hobby-Eberly Telescope (HET: Ramsey et al. 1998) using its High Resolution Spectrograph (HRS) (Tull 1998). The targets were selected according to the following criteria: 1) HET observability, with declination between  $-11^\circ$  and  $+72^\circ$ , and 2) Either a long-period ( $P \gtrsim 1$  yr) planet such that inner planets may be dynamically stable, or a very short-period ( $P \lesssim 10$  days) hot Jupiter which would allow for previously undetected outer planets, and 3) The orbital solution for the known planet in each system has RV residuals of  $10\text{-}20 \text{ m s}^{-1}$ , so that an additional planet may be present but undetected. The targets and their stellar parameters are listed in Table 1. Except where noted, masses are obtained from Takeda et al. (2007),  $[\text{Fe}/\text{H}]$ ,  $T_{\text{eff}}$ , and  $V \sin i$  from Valenti & Fischer (2005), and the chromospheric emission ratio  $\log R'_{HK}$  (Noyes et al. 1984) computed from measurements of the Ca II S-index obtained with the 2.7m telescope using the techniques developed by Paulson et al. (2002). The uncertainties on the stellar masses given in Takeda et al. (2007) are asymmetric about the central value; for the purposes of Table 1 and the determination of planetary parameters, the adopted stellar mass uncertainty was taken to be the larger of the two.

All of the HET observations for this program were performed at a spectral resolution of 60,000, with the 316 gr/mm cross-disperser and a central wavelength of  $5936\text{\AA}$ . An iodine cell temperature-controlled at  $70^\circ \text{C}$  was used as the velocity metric (Marcy & Butler 1992). This setup, identical to that used for the ongoing planet search program (Cochran et al. 2004; Endl et al. 2008), places the iodine region ( $\sim 5000\text{-}6000 \text{\AA}$ ) almost entirely onto the blue CCD, which is cosmetically superior to the red CCD. For each target, an iodine-free template spectrum was obtained near the beginning of the first season in which it was observable. We determined precise radial velocities following the general recipe outlined by Butler et al. (1996), using an advanced version of our own code “Austral” (Endl et al. 2000).

We observed each target with the HET in queue mode using a random observing interval of 2-10 days between visits. Each visit consisted of one spectrum, except for seven bright targets (HD 3651, HD 19994, HD 38529, HD 74156, 47 UMa, HD 128311, HD 136118) for which 3 consecutive spectra were obtained in each visit. HET data consisting of multiple exposures per visit were binned using the weighted mean value of the velocities in each visit. We adopted the quadrature sum of the rms about the mean and the mean internal error as the error bar of each binned point. This procedure was done for HD 3651, HD 19994, HD 38529, HD 74156, 47 UMa, HD 128311, and HD 136118. Targets were observed with the HET from 2004 December through 2007 November. During the three years of this study, supplemental observations were also made using the 2.7m Harlan J. Smith telescope at McDonald Observatory. All available published radial-velocity data were also gathered from the literature for the purpose of fitting orbits to the known planets. Those data are summarized in Table 2. All radial-velocity data obtained from McDonald Observatory are

given in Tables 10-45.

### 3. Refined Planetary System Parameters

#### 3.1. Orbit Fitting Results

Available published data were combined with velocities from the HET and the 2.7m to fit Keplerian orbits using GaussFit (Jefferys et al. 1987), which is a generalized least-squares program used here to solve a Keplerian radial-velocity orbit model. The GaussFit model has the ability to allow the offsets between data sets to be a free parameter. This is important because the radial velocities cited in published works, and those computed from HET and 2.7m data, are not absolute radial velocities, but rather are measured relative to the iodine-free stellar template. The Geneva planet-search group, however, makes use of a simultaneous thorium-argon calibration rather than an iodine absorption cell (Baranne et al. 1996). Each data set thus has an arbitrary zero-point offset which must be accounted for in the orbit-fitting procedure.

The best-fit Keplerian orbital solutions and planetary parameters are shown in Table 3. A summary of the fit results for each individual data set is given in Table 4. In computing the planetary minimum mass  $M \sin i$  and semimajor axis  $a$ , the stellar masses listed in Table 1 were used. The addition of a large amount of new data and the use of multiple independent data sets in fitting Keplerian orbits have generally improved the precision of the derived planetary parameters by a factor of 2-4 over the published results summarized in the Catalog of Nearby Exoplanets (Butler et al. 2006). In particular, the precision of the orbital periods have been improved by the addition of new data, due to the increased number of orbits now observed. Our parameters generally agree within  $2\sigma$  of previously published estimates. In this section, we highlight interesting results from the combined fits.

For each object, we searched for periodic signals in the residuals to the known planet’s orbit using a Lomb-Scargle periodogram (Lomb 1976; Scargle 1982). To assess the statistical significance of those periods, the false alarm probabilities (FAP) were calculated using the bootstrap randomization method detailed by Kürster et al. (1997). The bootstrap method randomly shuffles the velocity observations while keeping the times of observation fixed. The periodogram of this shuffled data set is then computed and its highest peak recorded. In this way, we can determine the probability that a periodogram peak of a given power level will arise by chance, without making any assumptions about the error distribution of the data. All bootstrap FAP estimates result from 10000 such realizations. Those results are shown in Table 5.

*HD 20367.* A planet orbiting HD 20367 was first announced in a conference proceedings (Udry et al. 2003), but has not yet appeared in a refereed journal. The Geneva planet search group website<sup>1</sup> lists the planet’s period as 469.5 days, with an eccentricity of 0.32 and  $M \sin i = 1.17 M_{\text{Jup}}$ . Eighty-one observations of HD 20367 were obtained with the HET over three observing seasons, as well as 19 observations from the 2.7m, but period searches of these data give no indication of such a signal.

Figure 1 shows the radial-velocity data from HET and the 2.7m telescopes, and the periodogram of those data. The Geneva group’s solution has been overplotted. The highest peak, at 5.58 days, has a bootstrap FAP of 8.5%. The dominant periodicity of 5.58 days, which was evident early in the observation campaign, prompted a photometric investigation to search for transits and to rule out stellar rotation. We obtained 132 observations of HD 20367 from 2006 September to 2007 January with the T10 0.8m automated photometric telescope (APT) at Fairborn Observatory in southern Arizona. The T10 APT and its precision photometer are very similar to the T8 APT described in Henry (1999). The precision of a single observation is typically around 0.001 mag. The results indicate a stellar rotation period of  $5.50 \pm 0.02$  days, with a photometric amplitude of  $0.0055 \pm 0.0003$  mag (Figure 2). From these observations, we conclude that the 5.6-day radial-velocity periodicity is caused by starspots rotating into and out of view. This is consistent with the estimate of  $P_{\text{rot}} = 6$  days reported by Wright et al. (2004), and the high level of chromospheric activity for this star ( $\log R'_{\text{HK}} = -4.50$ ). The literature contains conflicting age estimates for HD 20367: Holmberg et al. (2007) estimate an age of  $4.4^{+1.6}_{-2.1}$  Gyr, whereas Wright et al. (2004) report an age of 0.9 Gyr. Based on the rapid rotation rate, and the high level of chromospheric emission, the younger age estimate is favored.

The lack of any Keplerian signal in the 100 observations presented here leads us to conclude that there is not convincing evidence for the existence of HD 20367b.

*HD 74156.* For HD 74156, we fit the two planets at 51 and 2473 days using ELODIE and CORALIE data from Naef et al. (2004), and 82 independent HET visits. This system warrants closer scrutiny in light of the report by Bean et al. (2008) of a third planet, with a period of 346 days and a radial-velocity semi-amplitude  $K = 10.5 \text{ m s}^{-1}$ . That result was obtained using the same HET spectra as considered in this work, but velocities were derived using an independent method described in Bean et al. (2007). Here, we further investigate the possibility of an additional planet in the HD 74156 system. Applying our orbit-fitting methods as described above to the velocities for HD 74156 given in Bean et al. (2008), a periodogram peak is evident near 346 days, and we obtain a three-planet Keplerian orbit fit

---

<sup>1</sup><http://obswww.unige.ch/~udry/planet/hd20367.html>

which is consistent with that of Bean et al. (2008). This indicates that the fitting method used here is not responsible for our non-detection of HD 74156d.

It is possible that the HET velocities derived by Bean et al. (2008) are of superior quality to those presented here. However, the rms of the HET data about a two-planet fit reported by Bean et al. (2008) is  $8.5 \text{ m s}^{-1}$ , whereas we obtain an rms of  $8.3 \text{ m s}^{-1}$  for those data. These results suggest that there is no significant difference in quality between the two extant sets of HET velocities for HD 74156. The uncertainties quoted by Bean et al. (2008) are generally smaller than ours by a factor of 2-3. We repeated the fitting procedure, reducing the HET uncertainties by a factor of 2 and 3, but there was no significant change in the residuals: no signal is evident at periods near 346 days.

Since the total rms scatter about our two-planet fit is  $11.5 \text{ m s}^{-1}$ , and the semi-amplitude of planet d is  $K = 10.5 \text{ m s}^{-1}$ , it is possible that a third planetary signal may have been lost in the noise. To test this possibility, we performed the following Monte Carlo simulations. From each of the two data sets considered in the fits described here, we generated 1000 simulated sets of velocities consisting of three Keplerian signals plus a Gaussian noise term. This noise was equivalent to the mean uncertainty of each data set (ELODIE+CORALIE:  $10.8 \text{ m s}^{-1}$ , HET:  $8.3 \text{ m s}^{-1}$ ) added in quadrature to a stellar jitter of  $4 \text{ m s}^{-1}$  (the jitter estimate used in Bean et al. 2008). The parameters of the three simulated planets were those from Bean et al. (2008). These simulated datasets retained the times of observation and the error bars of the originals. We then fit the simulated data with a two-planet model exactly as described above, and examined the residuals of the two-planet fit by the periodogram method, to determine whether the signal of planet d was recovered. The criteria for recovery were that the period of the second planet had to be detected correctly and with a FAP of less than 0.1%. This FAP was computed using the analytic FAP formula of Horne & Baliunas (1986). Of the 1000 trials, only 11 did not result in a successful recovery of the signal of the second planet. The correct period was recovered 995 times, and the FAP exceeded 0.1% only 6 times; the worst FAP was 0.3%. These results indicate that our method should have been able to detect the signal of HD 74156d, had it been present with the parameters given by Bean et al. (2008).

In Bean et al. (2008), the iodine-free stellar template spectrum was obtained at a resolving power of  $R = 120,000$ , rather than the  $R = 60,000$  which is standard for targets in this paper. We obtained an  $R = 120,000$  template spectrum on 2007 Nov 12, but the velocities computed using this template resulted in a 2-planet fit with a slightly higher rms (HET:  $8.9 \text{ m s}^{-1}$ ) than the original  $R = 60,000$  template (HET:  $8.3 \text{ m s}^{-1}$ ). All analysis for HD 74156 in this paper refers to velocities obtained using the  $R = 60,000$  template.

A periodogram of the residuals to our 2-planet fit is shown in the left panel of Figure 3,

and those residuals are phased to the 346.6 day period in the right panel. The window function (grey dotted line) has a broad peak near 346 days due to the 1-year observing window. The phase gaps (right panel) are expected since the trial period is close to 1 year. No clear Keplerian signal is evident despite the large number of data points ( $N = 177$ ). We conclude from these data that there is not sufficient evidence for a third planet in the HD 74156 system.

*47 UMa (=HD 95128).* In Wittenmyer et al. (2007a), we performed these fits to an earlier set of data from McDonald Observatory. Those results did not provide convincing evidence for the outer planet reported by Fischer et al. (2002a) at  $P \sim 2594$  days; rather, we obtained a best-fit 2-planet model with  $P_2 \sim 6900$  days. Here we include an additional 14 epochs from HET, and the best-fit 2-planet model now calls for  $P_2 \sim 9660$  days. As in previous attempts to fit a second planet, the parameters  $e_2$  and  $\omega_2$  needed to be held fixed, at the values proposed by Fischer et al. (2002a):  $e_2 = 0.005$  and  $\omega_2 = 127^\circ$ . The rms about a single-planet model is  $10.2 \text{ m s}^{-1}$ , compared to  $8.6 \text{ m s}^{-1}$  when a second planet is included. Considering the continued ambiguity in the parameters for a second planet, and the ever-lengthening period of such an object, we use the one-planet fit for all further analysis in this work.

*HD 114783.* Vogt et al. (2002) reported the planet orbiting HD 114783, and recently, Wright et al. (2007) proposed an outer companion with a period of at least 8 yr. Here, we combine the Keck data given in Butler et al. (2006) with HET observations. A single-planet fit has a total rms of  $6.25 \text{ m s}^{-1}$  and  $\chi_\nu^2 = 4.91$ , whereas a two-planet fit reduces the rms to  $4.42 \text{ m s}^{-1}$  and the  $\chi_\nu^2$  to 1.81. The data considered in Wright et al. (2007) were of insufficient duration to establish a solution for the outer planet, but the combination of data allows for a Keplerian fit to converge. Although a 2-Keplerian model can be fit to these data, it is of limited utility: the outer planet has a 50% uncertainty in period ( $P_2 = 5098 \pm 2576$  days). Our results support those of Wright et al. (2007), that a second object is likely present, although there is not yet a sufficient time baseline of observations to establish its nature. The 1-planet fit was used to derive the parameters given in Table 3, and was also used for the detection-limits determination in § 5.

*HD 128311.* The inner planet ( $P \sim 450$  days) in the HD 128311 system was first discovered by Butler et al. (2003), who noted a linear trend in the residuals to the fit, as well as the extremely high activity level. Those authors estimated the stellar jitter at  $30 \text{ m s}^{-1}$ , and expressed concern that the planetary signal may have its origin in the stellar velocity jitter. Additional data proved that the inner planet was indeed real, and Vogt et al. (2005) reported a second planet at the 2:1 mean-motion resonance (MMR). They published a solution consisting of two superposed Keplerian orbits, noting that preliminary dynamical



tests showed the system to be unstable, and that the system was likely in a protected 2:1 resonance. Goździewski & Konacki (2006), in their dynamical analysis of available radial-velocity data, suggested that the observed signal could be attributed to a 1:1 resonance, i.e. a pair of Trojan planets. In this work, we fit a double Keplerian model to the combined Keck and HET data. Convergence is achieved, with a total rms of  $16.9 \text{ m s}^{-1}$  about both data sets (Keck– $15.8 \text{ m s}^{-1}$ , HET– $17.9 \text{ m s}^{-1}$ ). The residuals show a strong periodicity near 11.5 days, with bootstrap FAP less than 0.01%. Photometry of HD 128311 by G. Henry in Vogt et al. (2005) indicates a stellar rotation period of 11.53 days with a photometric amplitude of 0.03 mag. Hence, it is quite clear that the residual signal is caused by stellar rotation in this highly active star.

*HD 130322.* HD 130322 is host to a hot Jupiter in a 10.7-day period, discovered with the CORALIE observations of Udry et al. (2000). Four data sets are available for this object: CORALIE (Udry et al. 2000), Keck (Butler et al. 2006), HET, and 2.7m. Fitting all four sets together results in a total rms of  $14.8 \text{ m s}^{-1}$ , but removing the CORALIE data drops the rms to  $9.3 \text{ m s}^{-1}$ . In addition to the large scatter about the fit, a highly significant periodicity remains at 35 days (FAP<0.01%), which vanishes when the CORALIE data are removed. Due to these irregularities, we elect to exclude those data from the fits. The precision of the derived orbital parameters is not significantly affected by this removal, since the CORALIE data span only 167 days. For all further analysis in this work, we refer to the fit which excluded the CORALIE data. As given in Table 5, a residual period is present at  $P \sim 438$  days (FAP=0.16%). However, the HET velocities obtained using a second iodine-free template spectrum show no such periodicity. Those results show a residual period at 2.518 days, with a bootstrap FAP of 0.35%. A second planet can be fitted at this shorter period, and preliminary dynamical tests show that it would remain stable for at least  $10^7$  yr; however, the disagreement between the two templates makes it imprudent for us to claim a detection at this time.

#### 4. Dynamical Mapping

With the increasing availability of computing power and planetary systems, many investigators have undertaken N-body simulations of known planetary systems in an effort to characterise regions in which additional bodies could be found. Menou & Tabachnik (2003) performed a comprehensive test-particle analysis of 85 systems to determine the extent of the habitable zones in the presence of the known planet(s). Due to disruptions from the known giant planet’s “zone of influence,” they found that only one-fourth of the systems had dynamical habitability comparable to our own Solar system. In addition to test particles,

massive “test planets” have also been used to test observational claims for new planets and to probe known multiple-planet systems for additional regions of stability (Rivera & Lissauer 2000, 2001; Raymond & Barnes 2005; Rivera & Haghighipour 2007). Likewise, in this section we perform test-particle and massive-body simulations on the systems targeted by the intensive radial-velocity monitoring described in § 3.

#### 4.1. Test Particle Simulations

We performed test particle simulations using SWIFT<sup>2</sup> (Levison & Duncan 1994) to investigate the dynamical possibility of additional low-mass planets in each of the systems considered here. SWIFT is a numerical integration package which is designed to solve the equations of motion for gravitational interactions between massive bodies (star, planets) and massless test particles. Neptune-mass planets can be treated as test particles (1 Neptune mass = 0.054  $M_{\text{Jup}}$ ) since the exchange of angular momentum with jovian planets is small. We chose the regularized mixed-variable symplectic integrator (RMVS3) version of SWIFT for its ability to handle close approaches between massless, non-interacting test particles and planets. This version is most efficient when the gravitational interactions are dominated by a single body (the central star). A symplectic integrator has the advantage that errors in energy and angular momentum do not accumulate. Particles are removed if they are (1) closer than 1 Hill radius to the planet, (2) closer than 0.01 AU to the star, or (3) farther than 10 AU from the star. A planetary-mass object passing within 1 Hill radius of another planet, or within 0.01 AU ( $2 R_{\odot}$ ) of the star’s barycenter, is unlikely to survive the encounter. Since the purpose of these simulations is to determine the regions in which additional planets could remain in stable orbits, we set the outer boundary at 10 AU because the current repository of radial-velocity data cannot detect objects at such distances.

For each planetary system, 390 test particles were placed in initially circular orbits, spaced every 0.005 AU in the region between 0.05-2.0 AU. We have chosen to focus on this region because the duration of our high-precision HET data is currently 3-4 years for the objects in this study. The test particles were coplanar with the existing planet, which had the effect of confining the simulation to two dimensions. The initial orbital positions of the particles were randomly distributed in orbital phase with respect to the existing planets. The method used here are the same as Wittenmyer et al. (2007b), in which we performed test-particle simulations for six highly eccentric planetary systems. Input physical parameters (Table 3) for the known planet in each system were obtained from our Keplerian orbit fits

---

<sup>2</sup>SWIFT is publicly available at <http://www.boulder.swri.edu/~hal/swift.html>.

combining published velocity data and new observations from McDonald Observatory. The planetary masses were taken to be their minimum values ( $\sin i = 1$ ). By choosing the minimum mass for the planets, the regions of dynamical stability shown by the test-particle results are larger. Since the system inclinations are almost certainly not edge-on, and hence the true planetary masses are higher, we expect the actual regions of stability to be smaller than shown here. The systems were integrated for  $10^7$  yr, following Barnes & Raymond (2004) and allowing completion of the computations in a reasonable time. We observed that nearly all of the test-particle removals occurred within the first  $10^6$  yr; after this time, the simulations had essentially stabilized to their final configurations.

## 4.2. Test Particle Results

The results of the test-particle simulations are shown in Figures 4-13. The survival time of the test particles is plotted against their initial semimajor axis. Two systems targeted by the radial-velocity observations were not included in these simulations: HD 20367, because there is no evidence for a planet, and HD 128311, since the Keplerian orbit solution obtained in § 3.1 results in an unstable system. As shown in Figure 4, the short-period planet HD 3651b sweeps clean the region inside of about 0.5 AU. However, a small number of test particles remained in low-eccentricity orbits near the 1:3 and 2:1 mean-motion resonances (MMR). Since these regions lie within the orbital excursion of HD 3651b, these appear to be protected resonances. The eccentricity of the test particles in the region of the 1:3 MMR oscillated between 0.00 and 0.31 with a periodicity of about  $1.2 \times 10^5$  yr, while those in the 2:1 resonance remained at  $e \lesssim 0.07$  throughout the simulation. All particles beyond about 0.6 AU also remained in stable orbits, which is not surprising given the low mass of the planet. In simulations by Mandell et al. (2007) and Raymond et al. (2006), a migrating Jupiter-mass planet captured planetesimals into low-order resonances, and these accreted into terrestrial planets during the 200 Myr run. The architecture of the HD 3651 system, with a  $0.2 M_{\text{Jup}}$  planet at 0.3 AU, is similar to the configuration modeled by Mandell et al. (2007). Given the stable regions evident near the 1:3 and 2:1 resonances for HD 3651b, it is possible that terrestrial-mass planets were captured into these regions during the migration process. The detection limits for HD 3651 (§ 5) complement the dynamics well, and the current data can place upper limits of 1-2 Neptune masses (17-34 Earth masses) on such objects.

For most of the systems, the test-particle results give few surprises. Broad stable regions exist interior and exterior to HD 8574b, with the inner 0.47 AU retaining 100% of particles. For HD 10697 and HD 23596, particles remained in the inner 1.35 AU and 1.4 AU, respec-

tively. The HD 19994 system, shown in Figure 5, proved to be quite interesting. One would expect any particles in orbits which cross that of the planet to be removed straightaway, but a few particles remained near the 1:1 resonance with the planet, in the range 1.29-1.33 AU. Laughlin & Chambers (2002) investigated the possibility of planets in a 1:1 resonance, and concluded that such configurations are indeed possible. In the “eccentric resonance,” one 1:1 configuration described by Laughlin & Chambers (2002), one planet is in a nearly circular orbit while the other is in a highly eccentric orbit. Though the orbits cross, the longitudes of pericenter are sufficiently different to avoid close encounters.

In the HD 28185 system (Fig. 6), no stable regions exist exterior to the planet out to the maximum separation tested ( $a = 2.0$  AU). Figure 7 shows the results for the HD 38529 and HD 40979 systems. There is a broad region of stability between the widely-separated planets HD 38529b and c, consistent with the results of Barnes & Raymond (2004). The outer planet does not fall within the range of Fig. 7, but has an orbital excursion of 2.43–4.99 AU. For HD 74156, the recently-announced planet d (Bean et al. 2008) in a 346-day period between planets b and c, was not included in the simulation. Only those particles in a narrow strip near 1.25 AU survived the full 10 Myr; planet d would fall within the stable region.

The 47 UMa system (Figure 10) included only the inner planet ( $a = 2.11$  AU) for this experiment. The parameters of an outer planet are highly uncertain (Wittenmyer et al. 2007a; Naef et al. 2004), and such an object would be too distant to affect the inner 2 AU explored here. A large region interior to the planet is stable for the full duration, including the habitable zone. This result is consistent with that of Jones et al. (2001), who also found the 47 UMa habitable zone to be stable for an Earth-mass planet at 1 AU. With an  $M \sin i$  of  $6.9 M_{\text{Jup}}$ , HD 106252b clears out all particles outside of  $a \sim 0.7$  AU. For the HD 108874 system, no test particles survive between the two planets (Figure 11), but those in the innermost 0.3 AU remain stable. Particles interior to HD 114783b were stable to about  $a \sim 0.7$  AU. As expected for the HD 130322 hot-Jupiter system, all particles with  $a > 0.15$  AU survived (Fig. 12). In the HD 178911B system (Fig. 13, some particles remained in the inner 0.1 AU despite the large mass ( $M \sin i = 6.95 M_{\text{Jup}}$ ) and relative proximity ( $a = 0.34$  AU) of the planet.

### 4.3. Massive Body Simulations

Regions stable for massless test particles may not be stable for massive bodies. Alternatively, regions unstable for test particles may be able to host a massive planet. In the latter case, the existing planet(s) may adjust their orbits in response to the perturbation induced

by the introduced planet. For these reasons, it is important to also consider the effect of massive “test planets” in order to obtain a more complete dynamical picture of the systems under consideration. In this section, we explore the effect of inserting massive bodies into a known planetary system.

SWIFT’s RMVS3 integrator cannot handle close encounters, when massive bodies are closer to each other than 3 Hill radii. For the massive-body simulations, we use the Mercury orbital integrator (Chambers 1999), which has a hybrid feature that switches from an MVS integration to a Bulirsch-Stoer method when objects are within 3 Hill radii of each other. General relativistic effects have not been included. For these tests, fictitious planets were placed in each system on initially circular orbits at 0.05 AU intervals from 0.05-2.00 AU. The masses of the bodies were set at a Saturn mass ( $=0.3 M_{\text{Jup}}$ ); this is comparable to the mass detectable by the radial-velocity survey, and is the mass used by Raymond & Barnes (2005) in a similar investigation. These simulations ran for  $10^6$  yr, and we observed that unstable configurations usually resulted in system destruction within  $10^5$  yr. Figure 14 shows a histogram of the survival times for the unstable trials.

#### 4.4. Massive Body Results

The results of the massive-body simulations are shown in Figure 15. The filled circles indicate test planets which remained throughout the  $10^6$  yr integration. For most of the systems, the regions stable for test particles are also stable for Saturn-mass planets. For HD 3651 and HD 80606, some test planets which crossed orbits with the known planet survived. The 2:1 resonance of HD 3651b ( $a \sim 0.45$  AU) retained the Saturn-mass planet for  $10^6$  yr, although its eccentricity varied chaotically, reaching  $e \sim 0.22$ . The HD 80606 system gave the most unexpected result: Saturn-mass planets remained in the region  $a \leq 0.15$  AU, despite crossing orbits with HD 80606b. The test planets at 0.05, 0.10, and 0.15 AU reached maximum eccentricities of 0.13, 0.26, and 0.57, respectively. For the test planets at 0.05 and 0.10 AU, the oscillations in eccentricity were regular in period and constant in amplitude, whereas for  $a = 0.15$  AU, the oscillations varied in period and increased in amplitude toward the end of the  $10^6$  yr simulation (Figure 16). For the two cases in which the test planets exhibited irregular variations in eccentricity, the simulations were continued for  $10^7$  yr, anticipating the eventual destruction of the system. The test planet at 0.45 AU in the HD 3651 system caused the ejection of HD 3651b after  $1.8 \times 10^6$  yr. Likewise, the test planet at 0.15 AU in the HD 80606 system was ejected after  $5.7 \times 10^6$  yr.

## 5. Detection Limits

### 5.1. Methods

In Wittenmyer et al. (2006), we described a detection-limits algorithm implemented on the sample of constant stars from the long-term planet search at McDonald Observatory. This approach was based on that used by Endl et al. (2002) to derive detection limits from their survey with the ESO Coude Echelle Spectrometer. In brief, we add a Keplerian signal to the existing velocity data, then attempt to recover that signal using a Lomb-Scargle periodogram. The mass of the simulated planet is increased until 99% of the injected signals are recovered with  $\text{FAP} < 0.1\%$ . For the constant stars in Wittenmyer et al. (2006), the null hypothesis is that no planets are present, and so the detection-limit algorithm can be applied directly to the velocity data. In the case of the known planet hosts, this null hypothesis no longer applies, and it would not do to “pre-whiten” those data by removing the known planet’s orbit as if its parameters were known perfectly. The presence of an additional planet will act to modify the fitted parameters of the known planet. If two or more planets are present, and only one has been fitted, then part of the signal from the additional planets can be absorbed into the orbital elements of the 1-planet fit. To approach this task with the maximum rigor, these effects must be accounted for. Hence, the detection-limit algorithm was modified in the following way: the test Keplerian signal was added to each of the *original data sets*, then these modified data sets were fitted for the known planet(s) using GaussFit. A residuals file was generated and then subjected to the periodogram search as described above. This process of fitting and removing the known planet occurred for *every* injected test signal. This method has the advantage of being essentially identical to the planet-search method described in § 3.1.

### 5.2. Results

All data used in the fits for each planet host were subjected to the limits-determination routine, using 100 trial periods at even steps in the logarithm between 2 days and the total duration of observations. The results are plotted in Figures 17-27; planets with masses above the lines were recovered in 99% of trials (solid and dotted lines), or 50% of trials (dashed lines), and hence can be ruled out by the data at those confidence levels, respectively. To match the parameter space specifically targeted in this study, and to match that of the test-particle simulations, the detection-limits plots show the inner 2 AU only. For the eccentric trials (solid lines), the eccentricity of the injected test signals was chosen to be the mean eccentricity of the surviving test particles from the N-body simulations described in § 4.2.

This approach was chosen because the dynamical simulations demonstrated that objects placed in circular orbits do not stay that way; the eccentricity of an undetected low-mass planet is expected to be influenced to nonzero values by the known giant planet.

It is important to note that the limits presented here represent the companions that can be ruled out by the data with 99% confidence. Lower-mass planets could have been detected in this survey, but not necessarily at all (or 99% of all) possible configurations. It is likely that a particular combination of parameters for a simulated planet makes that signal fiendishly difficult to recover by this method, owing to the known planet’s radial-velocity signal and the sampling of the data. This is particularly important for simulated eccentric planets, where the velocity signal becomes markedly non-sinusoidal. The 50% limits are also shown to illustrate the effect of relaxing the recovery criteria in order to reduce the impact of especially unfortunate configurations.

Table 6 summarizes the results of the detection limits computations. The mean detection limits shown in Table 6 show that we could have detected 99% of planets with  $M \sin i \sim 1.6$  Neptune masses at 0.05 AU, and  $M \sin i \sim 2.4$  Neptune masses at 0.1 AU. The tightest limits were obtained for HD 3651, HD 108874, and 47 UMa, in which we are able to rule out Neptune-mass planets within 0.1 AU at the 99% level. For all of the systems, the limits shown in Figures 17-27 exhibit some “blind spots” evident where the periodogram method failed to recover the injected signals with  $FAP < 0.1\%$ . Typically this occurs at certain trial periods for which the phase coverage of the observational data is poor, and often at the 1-month and 1-year windows. Using this method of fitting the known planet for each injected trial signal, such regions of ignorance are also present at periods close to that of the existing planet.

## 6. Discussion

The aim of this project has been to intensively monitor known planetary systems in search of additional planets. However, in the sample of 22 planet hosts, the results have been quite the opposite. These new data cast doubt on the existence of two of the previously known planets, HD 20367b and 47 UMa c (Wittenmyer et al. 2007a). The announcement by Bean et al. (2008) of a third planet in the HD 74156 system, one of the targets of this study, prompted a detailed investigation; at present we cannot confirm this object. These results suggest that systems with multiple giant planets are considerably more rare, or harder to detect, than anticipated at the outset of this project.

In this section, we will explore some reasons why no new multiple-planet systems were

detected. Four possibilities are: 1) Biases in the target selection conspire against detection of weak signals, 2) There exist fundamental physical differences between single- and multiple-planet systems, 3) We did not obtain a sufficient quantity of high-quality data, and 4) Apparent single-planet systems may contain terrestrial-mass planets below the detection threshold.

### 6.1. Biases in the Sample

As with any scientific experiment, it is important to determine whether the sample selection resulted in unforeseen biases which affected the results. The target-selection process for this study, described in § 2, included an intentional bias in favor of planet hosts with “large” (10-20 m s<sup>-1</sup>) radial-velocity scatter about the orbital solution. The reasoning for this choice is straightforward: if a single planet can be fit with minimal scatter, there is little room for additional undetected planets to hide in the residuals. An unintended consequence of this selection criterion is that the excess scatter may be intrinsic to the star rather than indicative of additional planets. The achievable velocity precision improves with the number and strength of photospheric lines (Butler et al. 1996). Stars with higher temperatures or lower metallicities would have fewer and weaker lines, and result in lower velocity precision. In rapidly rotating stars, the spectral lines are broadened, which also degrades the radial-velocity precision. Fischer & Valenti (2005) showed that the probability of a given star hosting a planet is positively correlated with its metallicity. In addition, those authors suggested that among planet host stars, metal-rich stars are more likely to host multiple planets. To check for these sorts of biases, we can perform a Kolmogorov-Smirnov (K-S) test to determine the probability that two samples are drawn from the same distribution. Comparing our sample of 22 planet host stars with other planet hosts not targeted ( $N = 200$ ), the K-S test shows no significant differences in  $T_{eff}$  ( $P = 0.698$ ),  $[\text{Fe}/\text{H}]$  ( $P = 0.841$ ), or  $V \sin i$  ( $P = 0.323$ ). A comparison of the mean and median values of these quantities is shown in Table 7. The uncertainties are too large to make statistically meaningful comparisons, but the K-S test results suggest that there are no significant differences between the 22 planet hosts targeted here and those planet hosts not chosen.

### 6.2. Fundamental Differences

In this section, we ask the question, “Is there something special about the multi-planet systems”? Physical differences between single and multiple planet systems could arise either from the host star or from the processes of formation and dynamical evolution. Table 8 gives



statistics on the planetary and stellar parameters for single and multiple-planet systems. Only those planets detected by radial-velocity with  $M \sin i < 13 M_{\text{Jup}}$  were considered in the compilation of these statistics. Table 9 shows the results of K-S tests on the planetary and stellar characteristics listed in Table 8. None of the parameters tested showed statistically significant differences between single and multiple planet systems. There are hints from the data in Table 8, and the K-S test results in Table 9 that planets in multiple systems have larger  $a$  and smaller  $M \sin i$  than those in single-planet systems. Both of these trends would work against the radial-velocity detection of planets in multiple systems. As the semimajor axis  $a$  increases by a factor of  $N$ , the velocity semiamplitude  $K$  decreases by  $\sqrt{N}$ , and as the planet mass decreases by a factor of  $N$ ,  $K$  also drops by a factor of  $N$ . It is also possible that a tendency toward lower mass and larger semimajor axis in multi-planet systems is the result of a selection effect. Once a single planet is found, follow-up observations may reveal longer-period (larger  $a$ ) planets, and intensive monitoring programs such as this work may then find lower-mass planets. We can test whether a selection effect is at work by computing the statistics in Table 8 for the *first* planet discovered in the known multi-planet systems. These results are also given in Table 9; by comparing only the first planet found in the multiple systems with single planets, any significant difference between the distributions vanishes. Recently, Wright et al. (2008) have presented a detailed investigation of multiple-planet systems, and they find that planets in multiple systems tend to have lower eccentricities than single planets. We discuss this possibility in § 6.5. Wright et al. (2008) also note that the orbital distances of planets in multiple systems are more evenly distributed in log-period, whereas single planets are more frequent at  $a \sim 0.05$  AU and near 1 AU.

### 6.3. Observing Strategy

In considering whether there are important differences between the objects targeted in this work and known multi-planet systems, we can focus the comparison on the type of planetary system this survey was aimed at finding. The original motivation for this work was to investigate the possibility that systems containing a Jovian planet also contain Neptune-mass planets (1 Neptune mass =  $0.054 M_{\text{Jup}}$ ). At this writing, there are four such systems: 55 Cnc, GJ 876,  $\mu$  Ara (=HD 160691), and GJ 777A (=HD 190360). With a sample size of only four, a meaningful statistical comparison of the host stars is not possible, but one can look at the characteristics of the body of radial-velocity data for these systems. In so doing, we ask whether those data are of exceptional quality or quantity which facilitated the detection of the additional low-mass planets in those systems. The recent detection of a fifth planet in the 55 Cnc system by Fischer et al. (2008) used 636 measurements, binned into 250 Lick visits and 70 Keck visits. The detection of the fourth planet by McArthur et al. (2004)

used 138 HET observations combined with 143 Lick data points (Marcy et al. 2002) and 48 data points from Naef et al. (2004). For  $\mu$  Ara, the Neptune-mass planet was discovered using the HARPS spectrograph, which consistently delivers velocity precision of  $\sim 1 \text{ m s}^{-1}$  (Santos et al. 2004b; Pepe et al. 2007). The fourth planet in the  $\mu$  Ara system (Pepe et al. 2007) was discovered using a total of 86 HARPS measurements combined with data from CORALIE and the AAT. The  $18M_{\oplus}$  planet GJ 777Ac was discovered by Vogt et al. (2005) using 87 Keck velocities, and Rivera et al. (2005) found the  $7.5M_{\oplus}$  GJ 876d after 155 Keck observations. All four of these systems appear to have required an unusually large amount of the highest-quality data from Keck and HARPS, with a mean of 107 data points. By contrast, the targets in this work each received an average of 53 HET visits. It is possible that the number of visits required to detect a hot Neptune was underestimated.

#### 6.4. Swarms of Earths

Another possibility is that multiple-planet systems are indeed common, but, like our own Solar system, contain many terrestrial-mass objects which are undetectable by current radial-velocity surveys. Core-accretion simulations by Ida & Lin (2004a) predict a preponderance of  $1\text{-}10M_{\oplus}$  planets inside of 1 AU, and a “planet desert” in the range of  $10\text{-}100 M_{\oplus}$ , arising due to rapid gas accretion by cores once they reach about  $10 M_{\oplus}$ . The current survey is not sensitive to the terrestrial-mass objects, but planets within the “desert” could have been detected. Interestingly, Schlaufman et al. (2009) show that the presence of the planet desert could be confirmed by a radial-velocity survey with  $1 \text{ m s}^{-1}$  precision and  $\sim 700$  observations, which is similar in scope to the present work. Of course, many more than 22 systems need to be studied before conclusions can be made, but the characterization of hundreds of new systems by the *Kepler* spacecraft (Borucki et al. 2003) will help to define the upper and lower mass boundaries of the planet desert. Ida & Lin (2004a) note that the lower mass boundary would indicate the core mass required for rapid gas accretion, while the upper mass boundary would give insight into the mechanism by which gas accretion stops. *Kepler* discoveries of short-period super-Earths with masses  $1\text{-}10M_{\oplus}$  would lend further support to the core-accretion mechanism.

Simulations of planetesimal formation and migration also provide support for the existence of terrestrial-mass planets in systems with a gas giant planet. The GJ 876 system (Rivera et al. 2005), which contains two giant planets and an interior “super-Earth” ( $M \sin i = 7.5 M_{\oplus}$ ), is thought to have originated by the shepherding of material as the giant planets migrated inward (Zhou et al. 2005). 200 Myr simulations by Raymond et al. (2006) and Mandell et al. (2007) resulted in the formation of planets with 1-5 Earth masses interior

and exterior to the migrating hot Jupiter. Those models included only Type II migration, in which the migrating giant planet opens a gap in the protoplanetary disk. The models of Fogg & Nelson (2007) consider the effects of Type I migration, in which the giant planet does not open a gap in the disk and inward drift is driven by differential torques on the planet. Inclusion of Type I migration did not alter the general outcome, that planets of several Earth masses are shepherded inward by the hot Jupiter, and some remain exterior to it. These models indicate that the inner regions of planetary systems may be populated with terrestrial-mass planets which would remain wholly undetectable by current radial-velocity surveys. Although this work achieved detection limits of 15-30 Earth masses, rocky planets in the range of 1-5 Earth masses could easily have been missed.

### 6.5. Broader Implications for Planetary Systems

We now take a step back and look at the bigger picture of planetary system formation and evolution. Based on the target selection and the resulting detection limits, this survey was most sensitive to systems with two giant planets (larger than Saturn mass). More specifically, our “key demographic” is a system with a “cold” Jupiter ( $a \sim 1$  AU) and a close-in planet with  $M \sin i \gtrsim 1$ -2 Neptune masses ( $0.05$ - $0.1 M_{\text{Jup}}$ ). The detection limits given in § 5 exclude such configurations at the 99% level for all of the planetary systems considered here. Systems containing a long-period, massive planet could also have been detected by trends or curvature in the velocity residuals; no such trends were present for any of the targets. This survey was much less sensitive to planetary systems like our own, with multiple terrestrial-mass planets and long-period giants, for the reasons discussed in § 6.4. Planetary systems with architectures like our own Solar system may yet be common, but we will need to wait for the results from *Kepler* to begin making quantitative statements.

The results of this work are most useful in assessing the frequency of planetary systems in which extensive migration has occurred, to bring two gas giant planets interior to the “snow line.” In the core-accretion theory of giant planet formation (Pollack et al. 1996; Lissauer 1995), surface-density enhancement by ices facilitates the formation of  $\sim 10$ - $15 M_{\oplus}$  cores. The snow line, beyond which ices are present in the protoplanetary disk, has been estimated to lie at 1.6-1.8 AU in a minimum-mass solar nebula (Lecar et al. 2006). Perhaps the extensive migration required to construct systems with multiple giant planets with  $a \lesssim 2$  AU is uncommon; the typical timescale in which a system is undergoing migration may be short. In other words, migration may be fast, a hypothesis which has led to theoretical scenarios in which the observed planets are the last of many “batches” of planets which migrated onto the host star (Trilling et al. 2002; Ida & Lin 2004a; Narayan et al. 2005). Type I

migration, in which a net viscous torque on the protoplanet changes its orbit (Ward 1997), results in very fast migration with a timescale proportional to  $M_{planet}^{-1}$ . When a planet is massive enough ( $0.3-1.0 M_{Jup}$ ; Armitage 2007) to clear a gap in the disk, the slower Type II migration begins. The results of this work, showing a deficit of systems with multiple giant planets inside of 2-3 AU, suggest that they are dominated by Type I migration and rapidly accrete onto the star. Tanaka et al. (2002) showed that the Type I migration timescale is inversely proportional to the disk mass: planets in more massive disks migrate faster. If we make the reasonable assumption that multiple giant planets form from unusually massive disks, then Type I migration works against these planets surviving the migration if they remain below the gap-opening mass. To generate systems with multiple giant planets inside of 2-3 AU, migration should then be rapid enough to bring them there, but not so fast as to send the planets into the star. The results presented here suggest that such a scenario is uncommon.

In addition to migration, the dynamical history of planetary systems is an important factor in producing the observed architectures. The eccentricity distribution of extrasolar planets suggests that dynamically active histories are common. Interactions between giant planets can result in the ejection of one while imparting a significant eccentricity on the remaining planet (Rasio & Ford 1996; Ford et al. 2005; Malmberg & Davies 2008). Systems containing a single giant planet on a moderately eccentric orbit may be the result of such encounters, and thus less likely to host the sort of planets this survey was seeking. The median eccentricity of the planets targeted in this work is 0.29, compared to a median  $e$  of 0.15 for all other planets. Comparing the distributions by the K-S test gives a probability of 0.048, indicating a marginally significant difference between the two. Fischer et al. (2008) use the relatively low eccentricities ( $e < 0.2$ ) of the five 55 Cnc planets to suggest that a benign dynamical history allowed so many planets to remain. The GJ 876, HD 37124, HD 73526, and GJ 581 systems also have multiple planets with  $e < 0.2$ , but counterexamples are found in HD 160691, HD 74156, and HD 202206 ( $e_{max}=0.57, 0.64, \text{ and } 0.44$ , respectively). An uneventful dynamical history contributes to a planetary system’s observed end state, but comprises only a part of the picture in combination with its formation history.

A primary goal of the search for extrasolar planets is to estimate how common the architecture of our own Solar system might be. If the processes of planet formation and migration form many systems similar to our own, it becomes more likely that Earth-like planets may be present. The results of this work indicate that planetary systems like our own may be common if 1) terrestrial-mass planets are present but undetected, or 2) Type I migration timescales are so short that multiple giant planets rarely end up within 2-3 AU. Conversely, our Solar system may be rare if the dynamical history of most planetary systems results in many ejections and high eccentricities.

## 7. Summary

We have carried out an intensive radial-velocity campaign to monitor 22 known planetary systems for additional planets. No new planets were found, and these new data do not support the proposed planets HD 20367b, HD 74156d, and 47 UMa c. We have used test particles and Saturn-mass bodies to probe 20 planetary systems for regions in which additional planets could exist. The massive-body results are consistent with the test-particle results: each of these systems has regions, sometimes quite large, where additional planets may remain in stable orbits. Finally, we show that this campaign could have detected 99% of planets with  $M \sin i \lesssim 2.6$  Neptune masses within 0.10 AU.

This material is based on work supported by the National Aeronautics and Space Administration under Grants NNG04G141G, NNG05G107G issued through the Terrestrial Planet Finder Foundation Science program and Grant NNX07AL70G issued through the Origins of Solar Systems Program. We are grateful to the HET TAC for their generous allocation of telescope time for this project. Much of the computing for the dynamical simulations used the Lonestar cluster at the Texas Advanced Computing Center. This research has made use of NASA’s Astrophysics Data System (ADS), and the SIMBAD database, operated at CDS, Strasbourg, France. The Hobby-Eberly Telescope (HET) is a joint project of the University of Texas at Austin, the Pennsylvania State University, Stanford University, Ludwig-Maximilians-Universität München, and Georg-August-Universität Göttingen. The HET is named in honor of its principal benefactors, William P. Hobby and Robert E. Eberly.

## REFERENCES

- Baranne, A., et al. 1996, *A&AS*, 119, 373
- Barnes, R., Goździewski, K., & Raymond, S. N. 2008, *ApJ*, 680, L57
- Barnes, R., & Quinn, T. 2004, *ApJ*, 611, 494
- Barnes, R., & Raymond, S. N. 2004, *ApJ*, 617, 569
- Bean, J. L., McArthur, B. E., Benedict, G. F., & Armstrong, A. 2008, *ApJ*, 672, 1202
- Bean, J. L., McArthur, B. E., Benedict, G. F., Harrison, T. E., Bizyaev, D., Nelan, E., & Smith, V. V. 2007, *AJ*, 134, 749
- Bodenheimer, P., Hubickyj, O., & Lissauer, J. J. 2000, *Icarus*, 143, 2

- Bonfils, X., et al. 2007, *A&A*, 474, 293
- Borucki, W. J., et al. 2003, *Proc. SPIE*, 4854, 129
- Butler, R. P., Marcy, G. W., Vogt, S. S., Fischer, D. A., Henry, G. W., Laughlin, G., & Wright, J. T. 2003, *ApJ*, 582, 455
- Boss, A. P. 2003, *ApJ*, 599, 577
- Boss, A. P. 1998, *ApJ*, 503, 923
- Boss, A. P. 1995, *Science*, 267, 360
- Bouchy, F., et al. 2008, arXiv:0812.1608
- Butler, R. P., et al. 2006, *ApJ*, 646, 505
- Butler, R. P., Marcy, G. W., Williams, E., McCarthy, C., Dosanjuh, P., & Vogt, S. S. 1996, *PASP*, 108, 500
- Chambers, J. E. 1999, *MNRAS*, 304, 793
- Chatterjee, S., Ford, E. B., Matsumura, S., & Rasio, F. A. 2008, *ApJ*, 686, 580
- Cochran, W. D., et al. 2004, *ApJ*, 611, L133
- Cochran, W. D., Hatzes, A. P., & Hancock, T. J. 1991, *ApJ*, 380, L35
- Endl, M., Cochran, W. D., Wittenmyer, R. A., & Boss, A. P. 2008, *ApJ*, 673, 1165
- Endl, M., Kürster, M., & Els, S. 2000, *A&A*, 362, 585
- Endl, M., Kürster, M., Els, S. H. A. P., Cochran, W. D., Dennerl, K., Döbereiner, S. 2002, *A&A*, 392, 671
- Fischer, D. A., & Valenti, J. 2005, *ApJ*, 622, 1102
- Fischer, D. A., et al. 2008, *ApJ*, 675, 790
- Fischer, D. A., Marcy, G. W., Butler, R. P., Laughlin, G., & Vogt, S. S. 2002, *ApJ*, 564, 1028
- Fogg, M. J., & Nelson, R. P. 2007, *A&A*, 472, 1003
- Ford, E. B., Lystad, V., & Rasio, F. A. 2005, *Nature*, 434, 873

- Goździewski, K., & Konacki, M. 2006, *ApJ*, 647, 573
- Henry, G. W. 1999, *PASP*, 111, 845
- Holmberg, J., Nordström, B., & Andersen, J. 2007, *A&A*, 475, 519
- Horne, J. H., & Baliunas, S. L. 1986, *ApJ*, 302, 757
- Ida, S., & Lin, D. N. C. 2008, *ApJ*, 673, 487
- Ida, S., & Lin, D. N. C. 2004, *ApJ*, 604, 388
- Ida, S., & Lin, D. N. C. 2004, *ApJ*, 616, 567
- Jefferys, W. H., Fitzpatrick, M. J., & McArthur, B. E. 1987, *Celestial Mechanics*, 41, 39
- Jones, B. W., Sleep, P. N., & Chambers, J. E. 2001, *A&A*, 366, 254
- Jurić, M., & Tremaine, S. 2008, *ApJ*, 686, 603
- Kürster, M., Schmitt, J. H. M. M., Cutispoto, G., & Dennerl, K. 1997, *A&A*, 320, 831
- Latham, D. W., Stefanik, R. P., Mazeh, T., Mayor, M., & Burki, G. 1989, *Nature*, 339, 38
- Laughlin, G., & Chambers, J. E. 2002, *AJ*, 124, 592
- Lecar, M., Podolak, M., Sasselov, D., & Chiang, E. 2006, *ApJ*, 640, 1115
- Levison, H. F., & Duncan, M. J. 1994, *Icarus*, 108, 18
- Levison, H. F., Lissauer, J. J., & Duncan, M. J. 1998, *AJ*, 116, 1998
- Lissauer, J. J. 1995, *Icarus*, 114, 217
- Lomb, N. R. 1976, *Ap&SS*, 39, 447
- Lovis, C., et al. 2006, *Nature*, 441, 305
- Malmberg, D., & Davies, M. B. 2008, *arXiv:0811.3420*
- Mandell, A. M., Raymond, S. N., & Sigurdsson, S. 2007, *ApJ*, 660, 823
- Marcy, G. W., Butler, R. P., Fischer, D. A., Laughlin, G., Vogt, S. S., Henry, G. W., & Pourbaix, D. 2002, *ApJ*, 581, 1375
- Marcy, G. W., & Butler, R. P. 1992, *PASP*, 104, 270

- Mayor, M., et al. 2009, *A&A*, 493, 639
- Mayor, M., & Queloz, D. 1995, *Nature*, 378, 355
- Mayor, M., Udry, S., Naef, D., Pepe, F., Queloz, D., Santos, N. C., & Burnet, M. 2004, *A&A*, 415, 391
- Menou, K., & Tabachnik, S. 2003, *ApJ*, 583, 473
- McArthur, B. E., et al. 2004, *ApJ*, 614, L81
- Naef, D., Mayor, M., Beuzit, J. L., Perrier, C., Queloz, D., Sivan, J. P., & Udry, S. 2004, *A&A*, 414, 351
- Naef, D., et al. 2001, *A&A*, 375, L27
- Narayan, R., Cumming, A., & Lin, D. N. C. 2005, *ApJ*, 620, 1002
- Noyes, R. W., Hartmann, L. W., Baliunas, S. L., Duncan, D. K., & Vaughan, A. H. 1984, *ApJ*, 279, 763
- Paulson, D. B., Saar, S. H., Cochran, W. D., & Hatzes, A. P. 2002, *AJ*, 124, 572
- Pepe, F., et al. 2007, *A&A*, 462, 769
- Perrier, C., Sivan, J.-P., Naef, D., Beuzit, J. L., Mayor, M., Queloz, D., & Udry, S. 2003, *A&A*, 410, 1039
- Pollack, J. B., Hubickyj, O., Bodenheimer, P., Lissauer, J. J., Podolak, M., & Greenzweig, Y. 1996, *Icarus*, 124, 62
- Ramsey, L. W., et al. 1998, *Proc. SPIE*, 3352, 34
- Rasio, F. A., & Ford, E. B. 1996, *Science*, 274, 954
- Raymond, S. N., & Barnes, R. 2005, *ApJ*, 619, 549
- Raymond, S. N., Mandell, A. M., & Sigurdsson, S. 2006, *Science*, 313, 1413
- Rivera, E., & Haghighipour, N. 2007, *MNRAS*, 374, 599
- Rivera, E. J., & Lissauer, J. J. 2000, *ApJ*, 530, 454
- Rivera, E. J., & Lissauer, J. J. 2001, *ApJ*, 558, 392
- Rivera, E. J., et al. 2005, *ApJ*, 634, 625



- Santos, N. C., Israelian, G., & Mayor, M. 2004, *A&A*, 415, 1153
- Santos, N. C., et al. 2004, *A&A*, 426, L19
- Santos, N. C., Mayor, M., Naef, D., Pepe, F., Queloz, D., Udry, S., & Burnet, M. 2001, *A&A*, 379, 999
- Scargle, J. D. 1982, *ApJ*, 263, 835
- Schlaufman, K. C., Lin, D. N. C., & Ida, S. 2009, *ApJ*, 691, 1322
- Takeda, G., Ford, E. B., Sills, A., Rasio, F. A., Fischer, D. A., & Valenti, J. A. 2007, *ApJS*, 168, 297
- Tanaka, H., Takeuchi, T., & Ward, W. R. 2002, *ApJ*, 565, 1257
- Trilling, D. E., Benz, W., Guillot, T., Lunine, J. I., Hubbard, W. B., & Burrows, A. 1998, *ApJ*, 500, 428
- Trilling, D. E., Lunine, J. I., & Benz, W. 2002, *A&A*, 394, 241
- Tull, R. G. 1998, *Proc. SPIE*, 3355, 387
- Udry, S., et al. 2007, *A&A*, 469, L43
- Udry, S., Mayor, M., & Queloz, D. 2003, *Scientific Frontiers in Research on Extrasolar Planets*, 294, 17
- Udry, S., et al. 2000, *A&A*, 356, 590
- Valenti, J. A., & Fischer, D. A. 2005, *ApJS*, 159, 141
- Vogt, S. S., Butler, R. P., Marcy, G. W., Fischer, D. A., Henry, G. W., Laughlin, G., Wright, J. T., & Johnson, J. A. 2005, *ApJ*, 632, 638
- Vogt, S. S., Butler, R. P., Marcy, G. W., Fischer, D. A., Pourbaix, D., Apps, K., & Laughlin, G. 2002, *ApJ*, 568, 352
- Ward, W. R. 1997, *Icarus*, 126, 261
- Wittenmyer, R. A., Endl, M., & Cochran, W. D. 2007, *ApJ*, 654, 625
- Wittenmyer, R. A., Endl, M., Cochran, W. D., & Levison, H. F. 2007, *AJ*, 134, 1276
- Wittenmyer, R. A., Endl, M., Cochran, W. D., Hatzes, A. P., Walker, G. A. H., Yang, S. L. S., & Paulson, D. B. 2006, *AJ*, 132, 177

Wright, J. T., Upadhyay, S., Marcy, G. W., Fischer, D. A., Ford, E. B., & Johnson, J. A. 2008, arXiv:0812.1582

Wright, J. T., et al. 2007, ApJ, 657, 533

Wright, J. T., Marcy, G. W., Butler, R. P., & Vogt, S. S. 2004, ApJS, 152, 261

Zhou, J.-L., Aarseth, S. J., Lin, D. N. C., & Nagasawa, M. 2005, ApJ, 631, L85

Zucker, S., et al. 2002, ApJ, 568, 363

Table 1. Stellar Parameters

Star	Spec. Type	Distance (pc)	Mass ( $M_{\odot}$ )	[Fe/H]	$T_{eff}$ (K)	V sin $i$ (km s $^{-1}$ )	$\log R'_{HK}$
HD 3651	K0V	11.1±0.1	0.882±0.026	0.24±0.03	5221±44	1.1	-4.99±0.05
HD 8574	F8	44.2±1.6	1.122±0.022	-0.03±0.03	6050±44	4.5	-4.88±0.04
HD 10697	G5IV	32.6±0.9	1.112±0.026	0.17±0.03	5680±44	2.5	-5.07±0.15
HD 19994	F8V	22.4±0.4	1.365±0.042	0.27±0.03	6188±44	8.6	-4.93±0.04
HD 20367	G0	27.1±0.8	1.04±0.06 <sup>a</sup>	-0.09±0.10 <sup>b</sup>	5998±75	3.0	-4.50±0.05
HD 23596	F8V	52.0±2.3	1.159±0.062	0.33±0.03	5904±44	4.2	-4.96±0.05
HD 28185	G5	39.6±1.7	0.98±0.05 <sup>c</sup>	0.12±0.10 <sup>b</sup>	5546±75	3.0	-5.37±0.40
HD 38529	G4IV	42.4±1.7	1.477±0.052	0.51±0.03	5697±44	3.9	-5.01±0.03
HD 40979	F8V	33.3±0.9	1.154±0.028	0.15±0.03	6089±44	7.4	-4.59±0.01
HD 72659	G0V	51.4±2.7	1.068±0.022	-0.02±0.03	5920±44	2.2	-5.02±0.09
HD 74156	G0	64.6±4.6	1.238±0.044	0.11±0.03	6068±44	4.3	...
HD 80606	G5	58±20	0.958±0.072	0.47±0.03	5573±44	1.8	...
HD 89744	F7V	39.0±1.1	1.558±0.048	0.26±0.03	6291±44	9.5	-5.03±0.04
47 UMa	G0V	14.1±0.1	1.063±0.029	0.04±0.03	5882±44	2.8	-5.03±0.07
HD 106252	G0	37.4±1.3	1.007±0.024	-0.07±0.03	5870±44	1.9	-4.91±0.14
HD 108874	G5	68.5±5.8	0.950±0.036	0.19±0.03	5551±44	2.2	...
HD 114783	K0	20.4±0.4	0.853±0.034	0.21±0.03	5135±44	0.9	...
HD 128311	K0	16.6±0.3	0.828±0.012	0.08±0.03	4965±44	3.6	...
HD 130322	K0V	29.8±1.3	0.836±0.018	-0.02±0.03	5308±44	1.6	-4.76±0.02
HD 136118	F9V	52.3±2.3	1.191±0.026	-0.11±0.03	6097±44	7.3	-4.91±0.04
HD 178911B	G5	47±11	1.014±0.057	0.34±0.03	5668±44	1.9	-4.83±0.02
HD 190228	G5IV	62.1±3.1	1.821±0.050	-0.24±0.03	5348±44	1.9	-4.98±0.02

<sup>a</sup>Mass obtained from Holmberg et al. (2007).

<sup>b</sup>[Fe/H],  $T_{eff}$ , and V sin  $i$  obtained from Holmberg et al. (2007).

<sup>c</sup>Mass obtained from Santos et al. (2004a).

Table 2. Summary of Published Radial-Velocity Data

Star	Reference	$N$	$\langle \sigma \rangle$ ( $\text{m s}^{-1}$ )	RMS about fit ( $\text{m s}^{-1}$ )
HD 3651	Butler et al. (2006)	163	3.4	6.6
HD 8574	Perrier et al. (2003)	41	10.3	13.1
HD 8574	Butler et al. (2006)	26	10.4	23.0
HD 10697	Butler et al. (2006)	59	2.7	6.8
HD 19994	Mayor et al. (2004)	48	6.7	8.1
HD 23596	Perrier et al. (2003)	39	9.1	9.2
HD 28185	Santos et al. (2001)	40	6.5	10.0
HD 38529	Butler et al. (2006)	162	5.3	13
HD 40979	Butler et al. (2006)	65	9.1	23
HD 72659	Butler et al. (2006)	32	3.2	4.2
HD 74156	Naef et al. (2004)	95	10.8	10.6
HD 80606	Naef et al. (2001b)	61	13.7	17.7
HD 89744	Butler et al. (2006)	50	11.2	16.0
47 UMa	Fischer et al. (2002a)	91	5.7	7.4
47 UMa	Naef et al. (2004)	44	7.3	7.4
HD 106252	Perrier et al. (2003)	40	10.7	10.5
HD 106252	Butler et al. (2006)	15	11.4	9.1
HD 108874	Vogt et al. (2005)	49	3.4	3.7
HD 114783	Butler et al. (2006)	54	2.7	4.7
HD 128311	Vogt et al. (2005)	76	3.3	18.0
HD 130322	Udry et al. (2000)	118	12.4	16.1
HD 130322	Butler et al. (2006)	12	2.7	11.0
HD 136118	Butler et al. (2006)	37	16.1	22.0
HD 178911B	Zucker et al. (2002)	51	10.4	11.0
HD 178911B	Butler et al. (2006)	14	2.7	7.7
HD 190228	Perrier et al. (2003)	51	8.7	8.0

Table 3. Keplerian Orbital Solutions

Planet	Period (days)	$T_0$ (JD-2400000)	$e$	$\omega$ (degrees)	K (m s <sup>-1</sup> )	M sin $i$ (M <sub>Jup</sub> )	$a$ (AU)	$\chi^2_\nu$	rms m s <sup>-1</sup>
HD 3651 b	62.218±0.015	53932.6±0.6	0.596±0.036	242.5±4.5	15.9±0.7	0.229±0.008	0.295±0.003	3.82	6.3
HD 8574 b	227.0±0.2	53981.0±3.2	0.297±0.026	26.6±5.4	58.3±1.8	1.80±0.06	0.757±0.005	2.21	14.2
HD 10697 b	1075.2±1.5	51480±18	0.099±0.007	111.2±6.3	115.4±1.1	6.21±0.15	2.131±0.018	3.39	8.1
HD 19994 b	466.2±1.7	53757±72	0.063±0.062	346±55	29.3±2.1	1.37±0.12	1.305±0.016	5.27	14.0
HD 23596 b	1561±12	53163±22	0.266±0.014	272.6±3.3	127.0±2.0	7.71±0.39	2.772±0.062	0.88	8.7
HD 28185 b	385.9±0.6	53793.6±8.8	0.092±0.019	351.9±8.2	158.8±4.2	5.59±0.33	1.032±0.019	2.28	9.5
HD 38529 b	14.3098±0.0005	54012.64±0.16	0.257±0.015	92.5±3.9	56.1±0.9	0.839±0.030	0.131±0.002	6.32	11.8
HD 38529 c	2140.2±5.7	52256.4±6.4	0.341±0.005	17.8±1.2	173.2±1.2	13.38±0.39	3.712±0.048	6.32	11.8
HD 40979 b	264.15±0.23	53919.0±2.7	0.252±0.014	323.4±4.1	119.4±2.2	4.01±0.13	0.846±0.007	4.44	20.3
HD 72659 b	3383±100	51572±52	0.271±0.022	241±8	42.4±1.1	3.15±0.14	4.511±0.114	1.00	6.6
HD 74156 b <sup>a</sup>	51.645±0.003	53788.59±0.09	0.627±0.009	176.5±1.2	109.6±2.3	1.80±0.06	0.292±0.004	1.60	11.5
HD 74156 c	2473±13	53415±13	0.432±0.013	258.6±2.7	116.5±3.3	8.06±0.37	3.850±0.054	1.60	11.5
HD 80606 b	111.429±0.001	53421.923±0.004	0.9324±0.0006	300.4±0.3	470.6±1.8	3.91±0.19	0.447±0.011	1.41	13.3
HD 89744 b	256.78±0.05	51505.5±0.4	0.673±0.007	195.1±1.0	271.6±4.0	8.44±0.23	0.918±0.010	2.58	15.2
47 UMa b <sup>b</sup>	1076.6±2.3	49222±347	0.012±0.023	147±117	46.6±1.1	2.45±0.10	2.100±0.022	3.61	10.2
HD 106252 b	1531.0±4.7	53397.5±4.7	0.482±0.011	292.8±1.8	138.8±2.0	6.92±0.16	2.611±0.026	1.42	12.2
HD 108874 b	395.8±0.6	54069±17	0.082±0.021	232±10	37.0±0.8	1.29±0.06	1.038±0.014	0.88	4.1
HD 108874 c	1624±23	52839±44	0.239±0.031	27±10	18.2±0.7	0.99±0.06	2.659±0.060	0.88	4.1
HD 114783 b	493.7±1.8	53806±14	0.144±0.032	86±11	31.9±0.9	1.10±0.06	1.160±0.019	4.91	6.3
HD 128311 b	454.2±1.6	53835±11	0.345±0.049	63±16	46.5±4.5	1.45±0.13	1.086±0.008	21.38	16.9
HD 128311 c	923.8±5.3	56987±41	0.230±0.058	28±15	78.8±2.6	3.24±0.10	1.745±0.017	21.38	16.9
HD 130322 b <sup>c</sup>	10.7085±0.0003	53995.0±2.3	0.011±0.020	145±77	108.3±2.0	1.04±0.03	0.0896±0.0006	4.29	8.9
HD 136118 b	1187.3±2.4	52999.5±5.3	0.338±0.015	319.9±2.1	210.7±2.5	11.60±0.25	2.333±0.020	1.82	16.5
HD 178911B b	71.484±0.002	53808.1±0.3	0.114±0.003	168.2±1.6	343.3±1.0	7.03±0.28	0.339±0.006	1.80	9.1
HD 190228 b	1136.1±9.9	53522±12	0.531±0.028	101.2±2.1	91.4±3.0	5.93±0.20	2.604±0.032	0.78	7.4

<sup>a</sup>Results from two-planet fit.

<sup>b</sup>Results from one-planet fit.

<sup>c</sup>Results for HD 130322 exclude data from Udry et al. (2000).

Table 4. Summary of Radial-Velocity Data

Star	$N$	RMS about fit ( $\text{m s}^{-1}$ )	$\Delta T$ (days)	Source
HD 3651	163	6.5		Butler et al. (2006)
HD 3651	35	5.1		HET <sup>a</sup>
HD 3651	4	9.3		2.7m <sup>b</sup>
HD 3651 (total)	202	6.3	7376	
HD 8574	41	14.8		Perrier et al. (2003)
HD 8574	44	8.7		HET
HD 8574	16	13.4		2.7m
HD 8574	26	20.7		Butler et al. (2006)
HD 8574 (total)	128	14.2	3609	
HD 10697	59	6.5		Butler et al. (2006)
HD 10697	32	8.8		2.7m
HD 10697	40	9.7		HET
HD 10697 (total)	131	8.1	4057	
HD 19994	48	14.8		Mayor et al. (2004)
HD 19994	56	12.5		HET
HD 19994	12	18.5		2.7m
HD 19994 (total)	116	14.0	3367	
HD 20367 <sup>c</sup>	81	12.9		HET
HD 20367	19	10.5		2.7m
HD 20367 (total)	100	12.4	974	
HD 23596	39	9.4		Perrier et al. (2003)
HD 23596	63	8.5		HET
HD 23596	6	5.8		2.7m
HD 23596 (total)	108	8.7	3603	
HD 28185	40	10.4		Santos et al. (2001)
HD 28185	34	8.5		HET
HD 28185 (total)	74	9.5	2971	
HD 38529	162	13.0		Butler et al. (2006)
HD 38529	73	8.9		HET
HD 38529	7	9.2		2.7m
HD 38529 (total)	242	11.8	3745	
HD 40979	65	22.8		Butler et al. (2006)
HD 40979	91	18.9		HET
HD 40979	4	9.6		2.7m
HD 40979 (total)	160	20.3	3588	
HD 72659	32	4.1		Butler et al. (2006)
HD 72659	53	7.8		HET
HD 72659 (total)	85	6.6	3593	
HD 74156	95	13.8		Naef et al. (2004)
HD 74156	82	8.3		HET
HD 74156 (total)	177	11.5	3408	
HD 80606	61	18.6		Naef et al. (2001b)
HD 80606	23	6.1		HET
HD 80606	46	5.3		Butler et al. (2006)
HD 80606 (total)	130	13.3	2893	
HD 89744	50	16.2		Butler et al. (2006)

Table 4—Continued

Star	$N$	RMS about fit ( $\text{m s}^{-1}$ )	$\Delta T$ (days)	Source
HD 89744	33	12.9		HET
HD 89744	9	19.0		2.7m
HD 89744 (total)	92	15.2	2943	
47 UMa	91	11.1		Fischer et al. (2002a)
47 UMa	44	11.8		Naef et al. (2004)
47 UMa	43	11.4		2.7m
47 UMa	77	7.0		HET
47 UMa (total)	255	10.2	7673	
HD 106252	40	14.8		Perrier et al. (2003)
HD 106252	43	8.2		HET
HD 106252	15	12.2		Butler et al. (2006)
HD 106252	12	16.1		2.7m
HD 106252 (total)	110	12.2	3682	
HD 108874	49	3.4		Vogt et al. (2005)
HD 108874	40	4.8		HET
HD 108874 (total)	89	4.1	2850	
HD 114783	54	6.6		Butler et al. (2006)
HD 114783	34	5.8		HET
HD 114783 (total)	88	6.3	3208	
HD 128311	76	15.8		Vogt et al. (2005)
HD 128311	78	17.9		HET
HD 128311 (total)	154	16.9	3335	
HD 130322	12	8.3		Butler et al. (2006)
HD 130322	30	8.7		HET
HD 130322	5	13.3		2.7m
HD 130322 (total)	47	8.9	2496	
HD 136118	37	21.6		Butler et al. (2006)
HD 136118	64	18.3		HET
HD 136118	4	14.9		2.7m
HD 136118 (total)	108	16.5	3450	
HD 178911B	51	11.5		Zucker et al. (2002)
HD 178911B	40	5.4		HET
HD 178911B	14	7.5		Butler et al. (2006)
HD 178911B (total)	105	9.1	3392	
HD 190228	51	8.8		Perrier et al. (2003)
HD 190228	42	9.8		HET
HD 190228	8	9.3		2.7m
HD 190228 (total)	101	9.2	3776	

<sup>a</sup>9.2 m Hobby-Eberly Telescope.

<sup>b</sup>McDonald Observatory 2.7 m Harlan J. Smith Telescope.

<sup>c</sup>No planet was fit.

Table 5. Results of Periodogram Analysis

Star	Period (days)	FAP
HD 3651	44.17	0.707
HD 8574	2272.73	0.687
HD 10697	26.68	0.028
HD 19994	54.88	0.399
HD 20367	5.58	0.085
HD 23596	25.13	0.141
HD 28185	4.76	0.224
HD 38529	294.12	0.023
HD 40979	2.26	0.795
HD 72659	6.99	0.758
HD 74156	80.39	0.035
HD 80606	357.14	0.616
HD 89744	23.27	0.075
47 UMa <sup>a</sup>	2380.95	0.045
47 UMa <sup>b</sup>	2.91	0.341
HD 106252	322.58	0.126
HD 108874	12.39	0.857
HD 114783	8.44	0.925
HD 128311	11.21	<0.0001
HD 130322	438.60	0.002
HD 136118	442.48	0.014
HD 178911B	7.88	0.925
HD 190228	2.57	0.777

<sup>a</sup>Residuals from one-planet fit.

<sup>b</sup>Residuals from two-planet fit.



Table 6. Companion Limit Summary

Star	Eccentricity	M sin $i$ 0.05 AU ( $M_{\text{Jup}}$ )	M sin $i$ 0.1 AU ( $M_{\text{Jup}}$ )	Median $K$ 99% recovery $\text{m s}^{-1}$	Median $K$ 50% recovery $\text{m s}^{-1}$
HD 3651	0.20	0.025	0.041	4.8	...
HD 3651	0	0.024	0.040	4.4	3.2
HD 8574	0.10	0.124	0.142	14.1	...
HD 8574	0	0.124	0.143	14.1	10.2
HD 10697	0.04	0.059	0.094	7.4	...
HD 10697	0	0.059	0.094	7.4	5.6
HD 19994	0.09	0.116	0.173	16.2	...
HD 19994	0	0.117	0.166	16.2	10.7
HD 20367	0	0.098	0.122	12.3	9.3
HD 23596	0.10	0.081	0.091	8.5	...
HD 23596	0	0.078	0.092	8.5	6.4
HD 28185	0.09	0.083	0.129	12.3	...
HD 28185	0	0.080	0.129	11.7	9.7
HD 38529	0.12	0.078	0.123	8.9	...
HD 38529	0	0.075	0.124	8.9	5.8
HD 40979	0.11	0.135	0.201	17.8	...
HD 40979	0	0.123	0.193	17.0	12.3
HD 72659	0.10	0.057	0.085	8.1	...
HD 72659	0	0.054	0.085	8.1	5.6
HD 74156	0.15	0.080	0.109	10.7	...
HD 74156	0	0.074	0.105	10.2	7.4
HD 80606	0.31	0.119	0.184	18.7	...
HD 80606	0	0.104	0.160	15.5	10.2
HD 89744	0.01	0.176	0.197	18.7	...
HD 89744	0	0.168	0.197	18.7	12.9
47 UMa	0.02	0.039	0.067	6.1	...
47 UMa	0	0.039	0.067	6.1	4.6
HD 106252	0.15	0.091	0.179	12.9	...
HD 106252	0	0.087	0.173	12.3	9.3
HD 108874	0.15	0.035	0.059	5.8	...
HD 108874	0	0.034	0.055	5.6	3.5
HD 114783	0.11	0.056	0.083	8.5	...
HD 114783	0	0.056	0.080	8.1	6.1
HD 128311	0	0.102	0.166	16.2	12.9
HD 130322	0.02	0.147	0.231	22.5	...
HD 130322	0	0.147	0.231	22.5	13.5
HD 136118	0.11	0.125	0.224	16.2	...
HD 136118	0	0.120	0.226	16.2	12.9
HD 178911B	0.07	0.061	0.130	10.2	...
HD 178911B	0	0.066	0.124	9.7	7.0
HD 190228	0.16	0.080	0.114	8.1	...
HD 190228	0	0.077	0.110	7.7	5.8
Mean (99% recovery)	0	0.087±0.036	0.131±0.052		
Mean (50% recovery)	0	0.063±0.027	0.090±0.036		

Table 6—Continued

Star	Eccentricity	M sin $i$ 0.05 AU (M <sub>Jup</sub> )	M sin $i$ 0.1 AU (M <sub>Jup</sub> )	Median $K$ 99% recovery m s <sup>-1</sup>	Median $K$ 50% recovery m s <sup>-1</sup>
------	--------------	---	--	---	---

Table 7. Comparison of Stellar Characteristics

Quantity	Targets	Non-Targets	Units
[ $Fe/H$ ] (mean)	0.12±0.18	0.07±0.23	dex
[ $Fe/H$ ] (median)	0.13	0.14	dex
$T_{eff}$ (mean)	5741±361	5608±496	K
$T_{eff}$ (median)	5697	5704	K
( $B - V$ ) (mean)	0.67±0.11	0.74±0.20	mag
( $B - V$ ) (median)	0.63	0.69	mag
V sin $i$ (mean)	3.72±2.50	2.75±1.72	km s <sup>-1</sup>
V sin $i$ (median)	2.48	2.40	km s <sup>-1</sup>

Table 8. Characteristics of Single and Multiple Planet Systems

Quantity	Single	Multiple	Units
$a$ (mean)	0.95±1.05	1.19±1.38	AU
$a$ (median)	0.49	0.63	AU
$e$ (mean)	0.24±0.23	0.19±0.17	
$e$ (median)	0.18	0.16	
M sin $i$ (mean)	2.72±3.16	1.93±2.38	M <sub>Jup</sub>
M sin $i$ (median)	1.60	1.03	M <sub>Jup</sub>
Star mass (mean)	1.14±0.41	1.06±0.32	M <sub>⊙</sub>
Star mass (median)	1.07	1.04	M <sub>⊙</sub>
[ $Fe/H$ ] (mean)	0.09±0.21	0.05±0.30	dex
[ $Fe/H$ ] (median)	0.14	0.14	dex
$T_{eff}$ (mean)	5640±473	5532±529	K
$T_{eff}$ (median)	5724	5584	K
( $B - V$ ) (mean)	0.73±0.18	0.77±0.22	mag
( $B - V$ ) (median)	0.68	0.72	mag

Table 9. K-S Tests on Single and Multiple Planet Systems

Quantity	K-S Probability <sup>a</sup>
$a$	0.004
$a$ (first planet)	0.249
$M \sin i$	0.015
$M \sin i$ (first planet)	0.349
$e$	0.125
Star mass	0.644
$[Fe/H]$	0.841
$T_{eff}$	0.135
$(B - V)$	0.383

<sup>a</sup>Probability that the two samples are drawn from the same distribution.

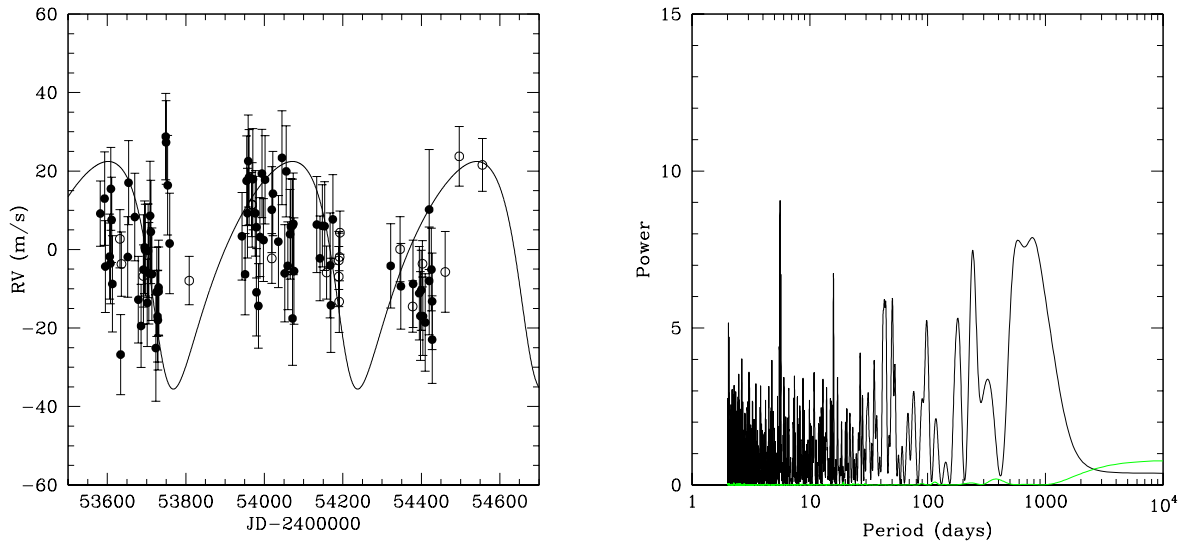


Fig. 1.— Left panel: Radial-velocity data for HD 20367. Filled circles: HET, open circles: 2.7m. The Geneva group’s orbital solution for the proposed planet is shown as a solid line. Right panel: Lomb-Scargle periodogram of the velocities. The 5.5-day stellar rotation period is evident, but no other periodicities are significant.

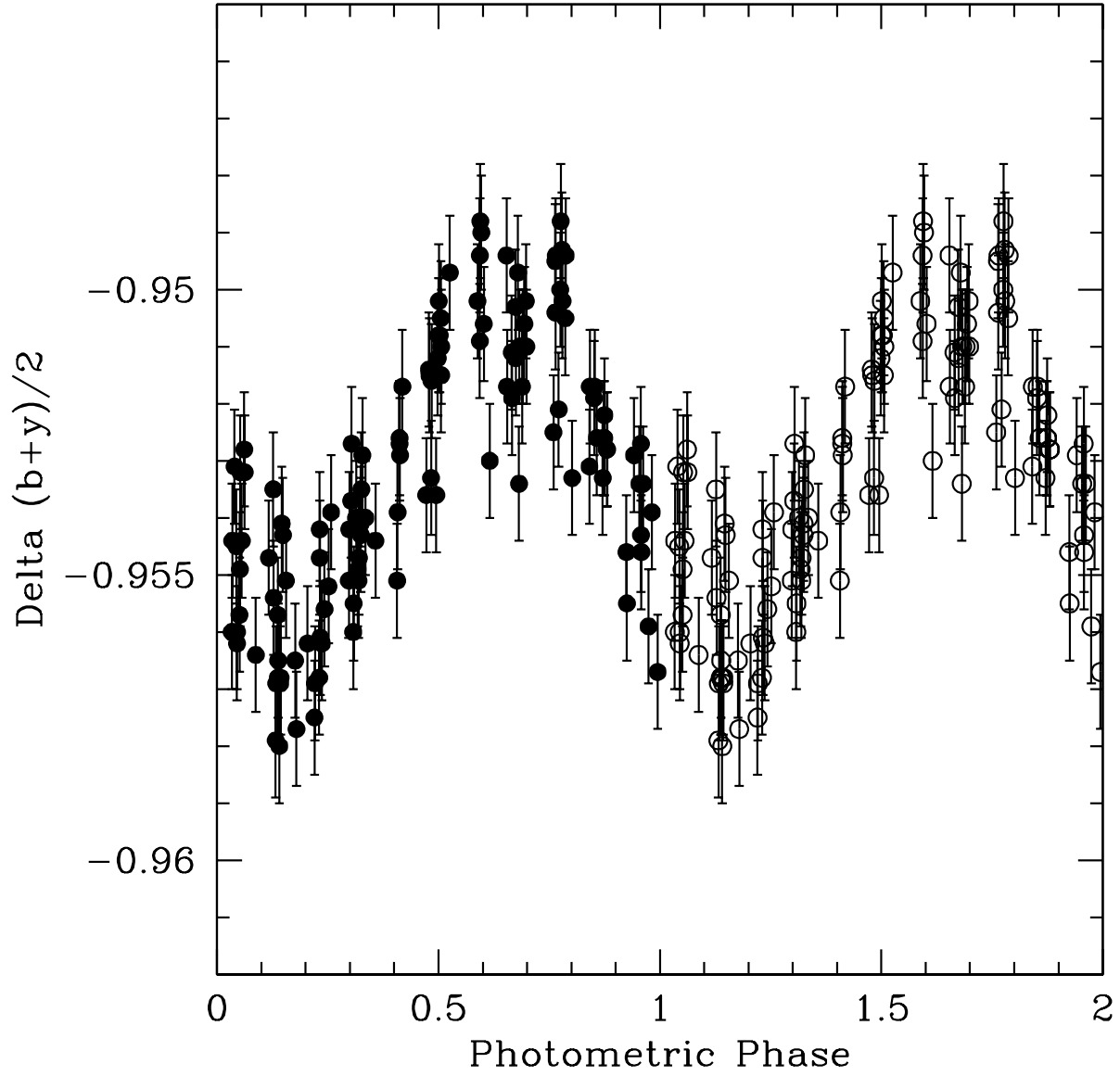


Fig. 2.— Photometric observations of HD 20367 phased to the stellar rotation period of 5.50 days. Two cycles are shown for clarity.

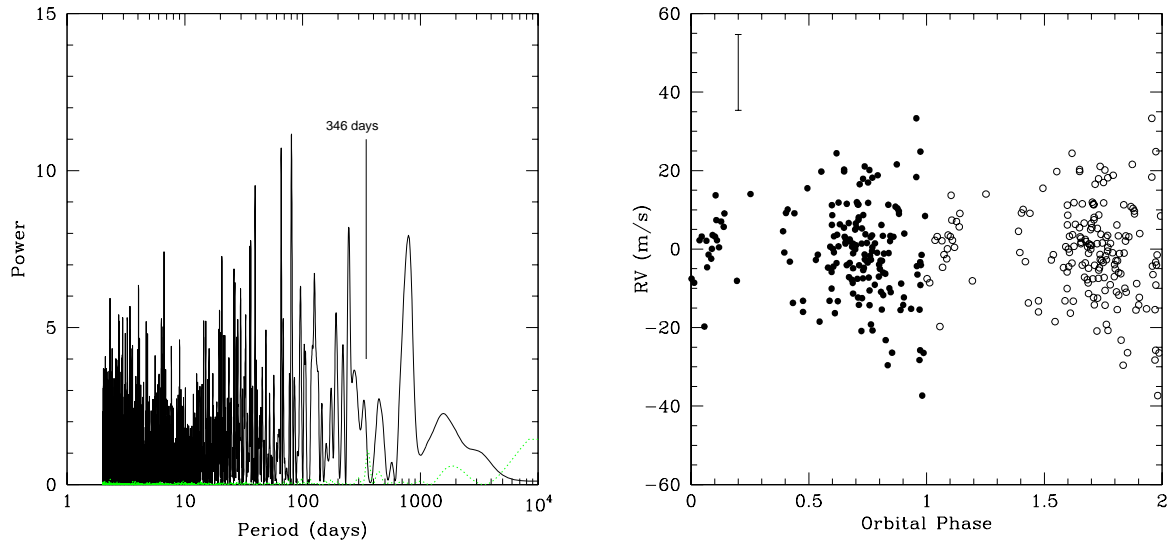


Fig. 3.— Left panel: Periodogram of the residuals of a 2-planet fit for the HD 74156 system. The window function is shown as a grey dotted line, and the 346-day period of planet d is marked. Right panel: The residuals to the 2-planet fit, phased to a period of 346.6 days (Bean et al. 2008). For clarity, two cycles are shown, and the error bars have been omitted. A reference error bar representing the mean uncertainty of  $9.65 \text{ m s}^{-1}$  is shown.

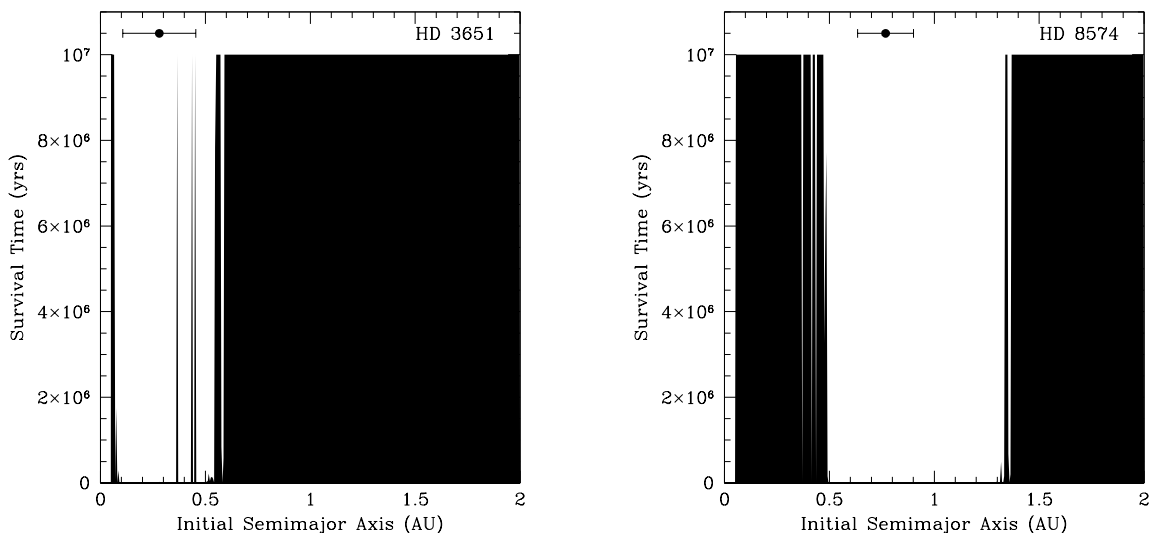


Fig. 4.— Left panel: Survival time as a function of initial semimajor axis for test particles in the HD 3651 system after  $10^7$  yr. The filled regions indicate test particles which survived. The orbital excursion of HD 3561b is indicated by the horizontal error bars at the top. Particles were placed on initially circular orbits with  $0.05 < a < 2.00$  AU. Right panel: Same, but for the HD 8574 system.

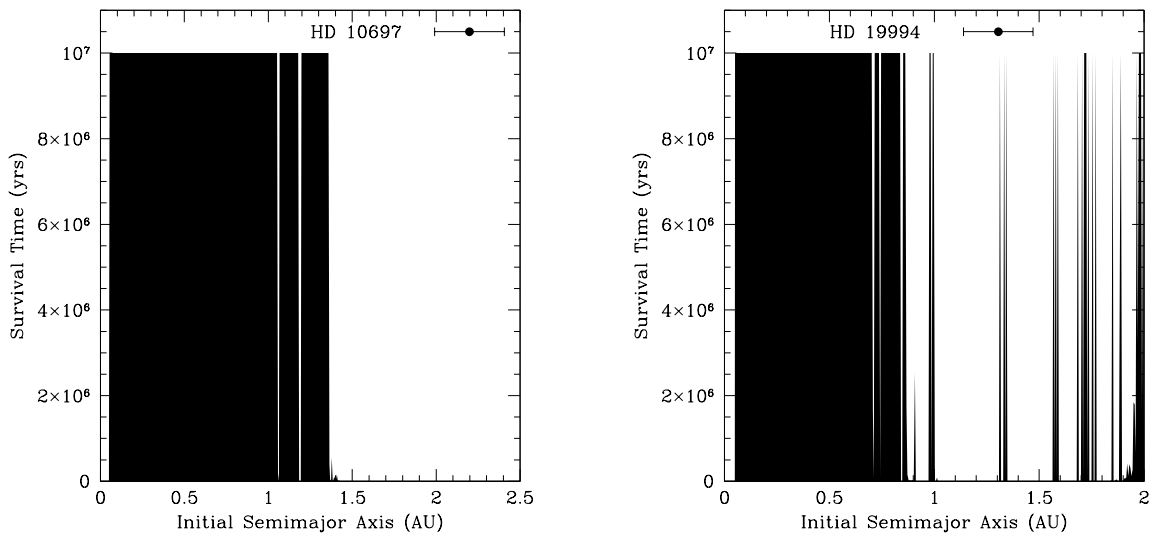


Fig. 5.— Same as Fig. 4, but for the HD 10697 (left) and HD 19994 (right) systems.

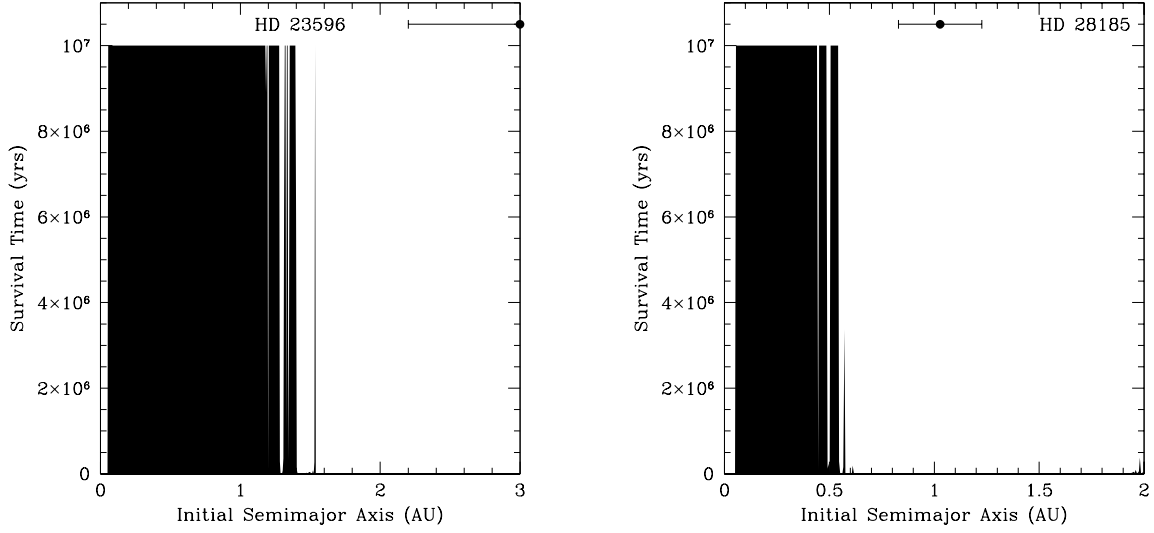


Fig. 6.— Same as Fig. 4, but for the HD 23596 (left) and HD 28185 (right) systems.

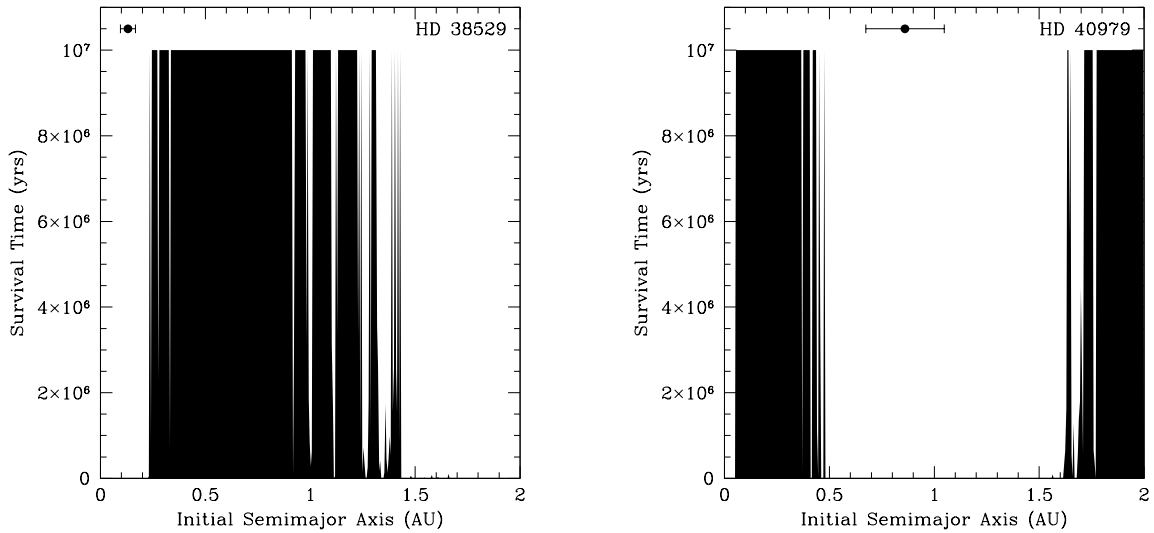


Fig. 7.— Same as Fig. 4, but for the HD 38529 (left) and HD 40979 (right) systems.



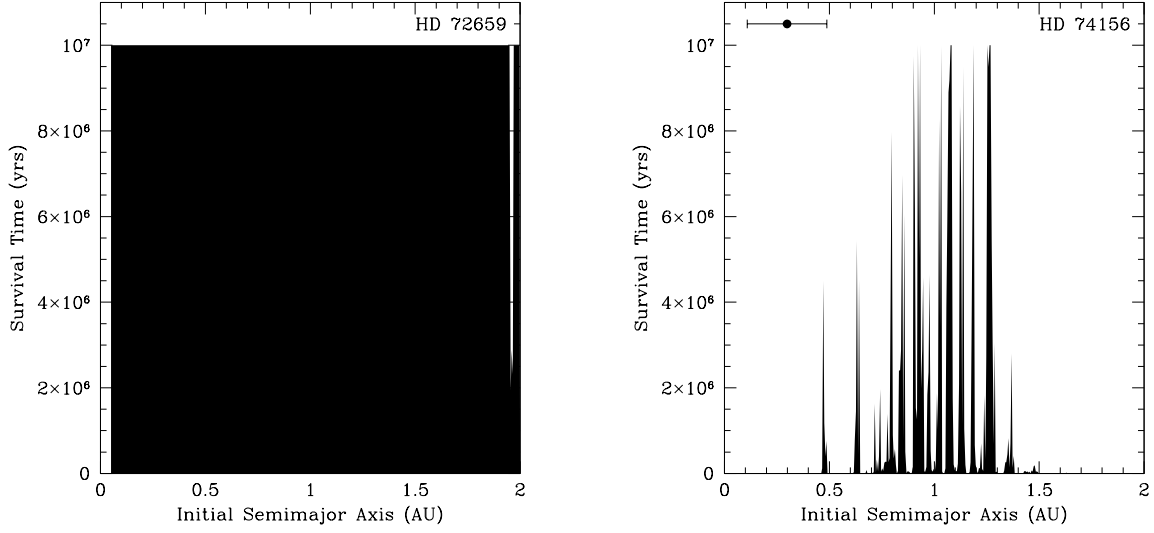


Fig. 8.— Same as Fig. 4, but for the HD 72659 (left) and HD 74156 (right) systems. HD 72659b, with an orbital excursion of 3.48–6.48 AU, is off the plot. The recently-announced planet HD 74156d, between planets b and c, was not included in the simulation, but would reside in the narrow stable strip.

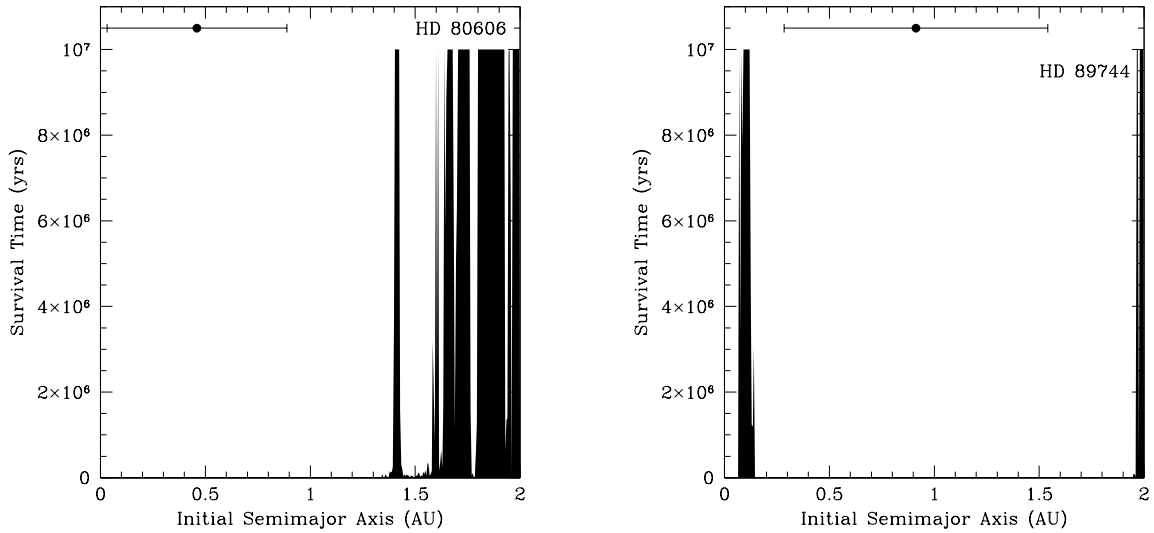


Fig. 9.— Same as Fig. 4, but for the HD 80606 (left) and HD 89744 (right) systems.

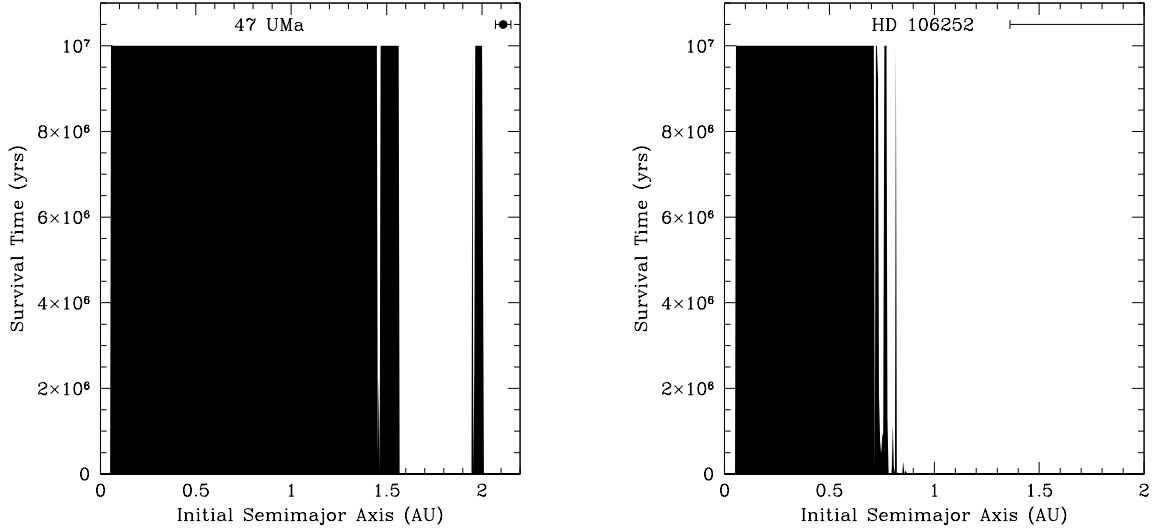


Fig. 10.— Same as Fig. 4, but for the 47 UMa (left) and HD 106252 (right) systems. Only 47 UMa b was considered in the simulations. An outer body would be too distant to affect the region under consideration.

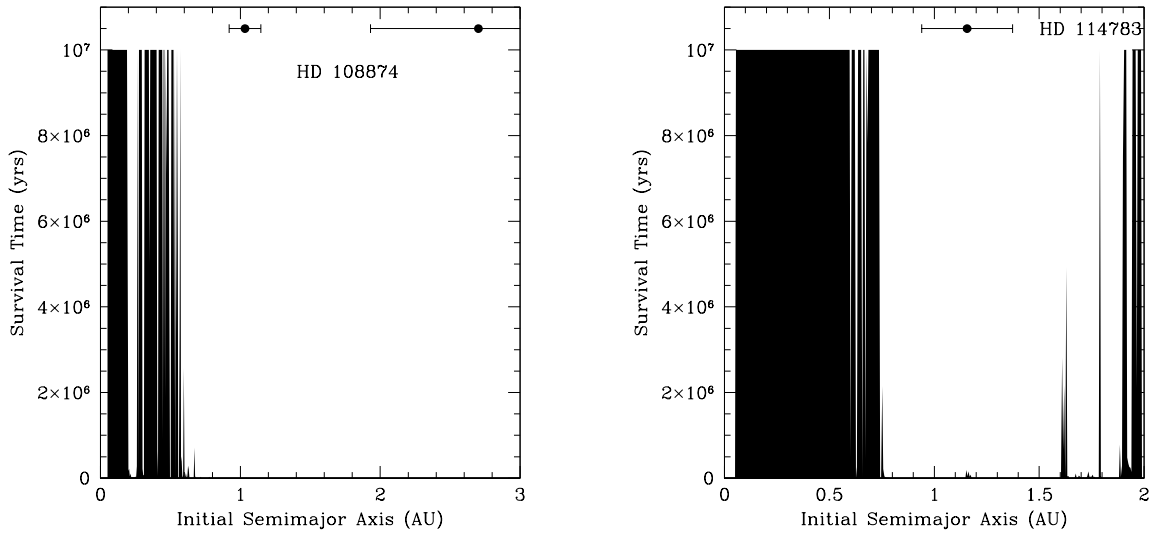


Fig. 11.— Same as Fig. 4, but for the HD 108874 (left) and HD 114783 (right) systems.

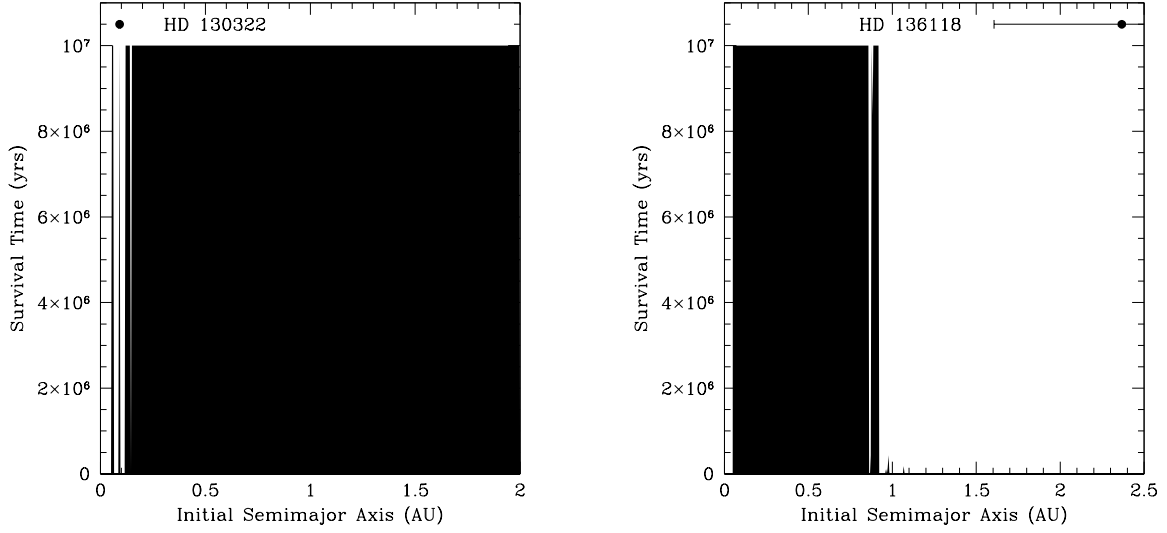


Fig. 12.— Same as Fig. 4, but for the HD 130322 (left) and HD 136118 (right) systems.

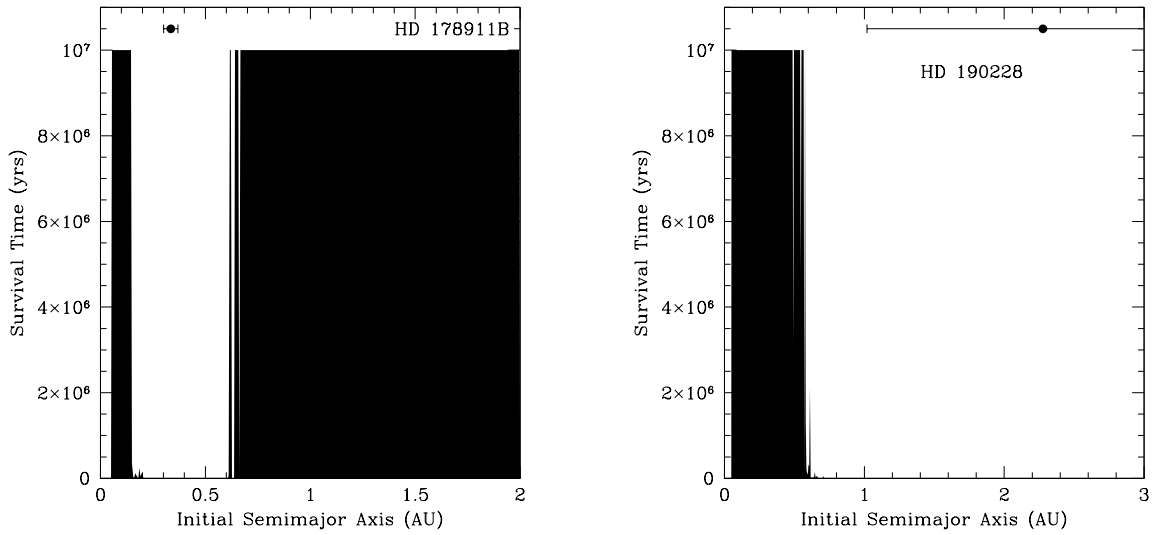


Fig. 13.— Same as Fig. 4, but for the HD 178911B (left) and HD 190228 (right) systems.

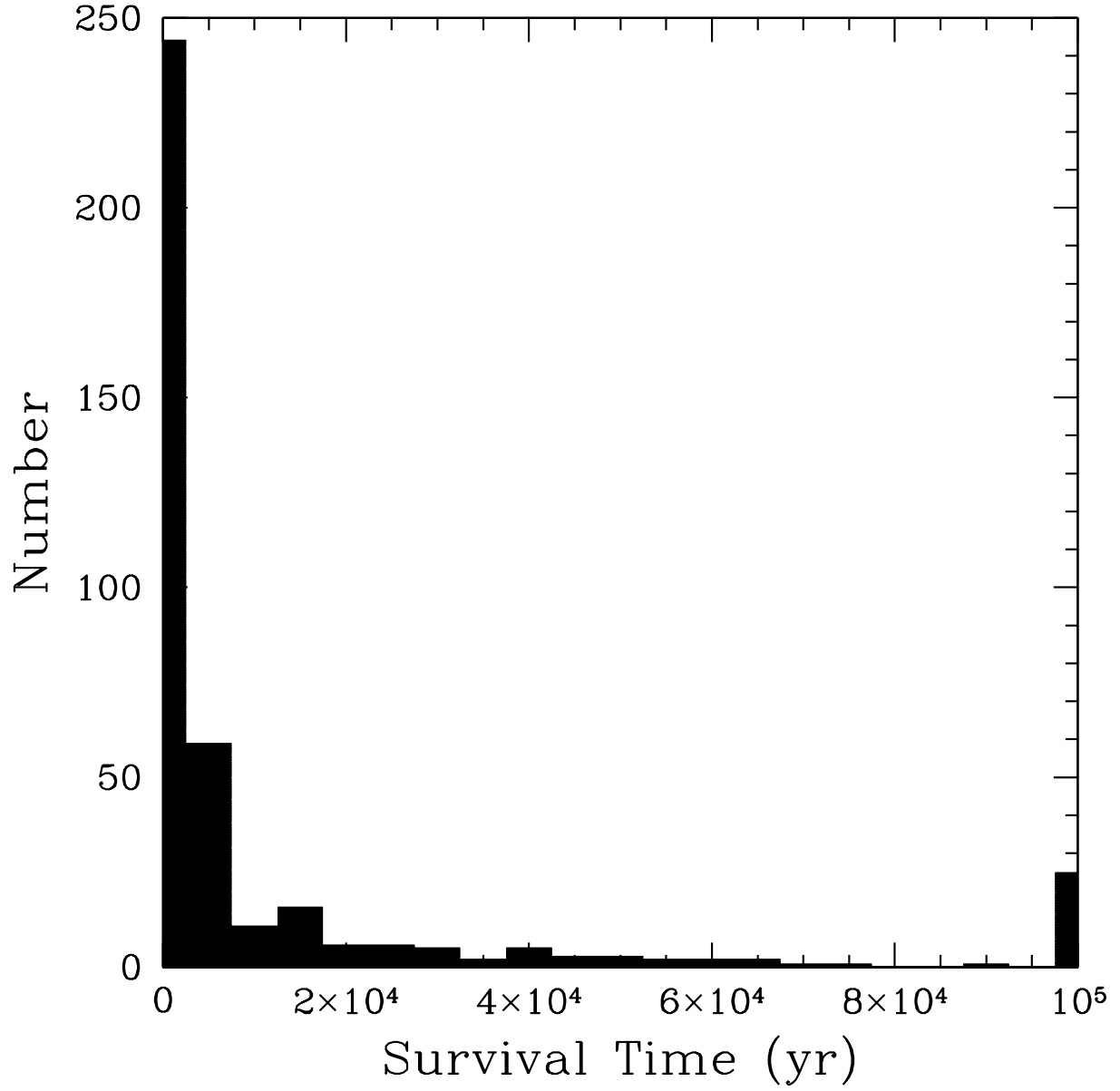


Fig. 14.— Histogram of the survival times for the unstable test configurations ( $N = 352$ ). Twenty realizations survived longer than  $10^5$  yr.

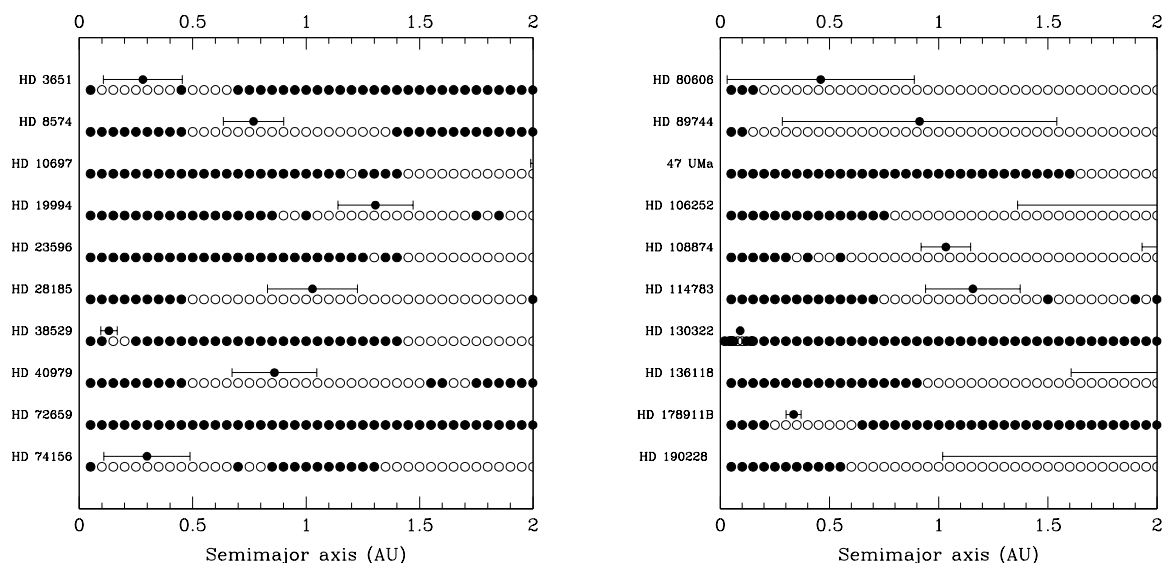


Fig. 15.— Survival of Saturn-mass planets for  $10^6$  yr on initially circular orbits in 20 planetary systems. The orbital excursions of the existing planets are indicated by the horizontal error bars. Open circles represent unstable locations, filled circles were stable for  $10^6$  yr.

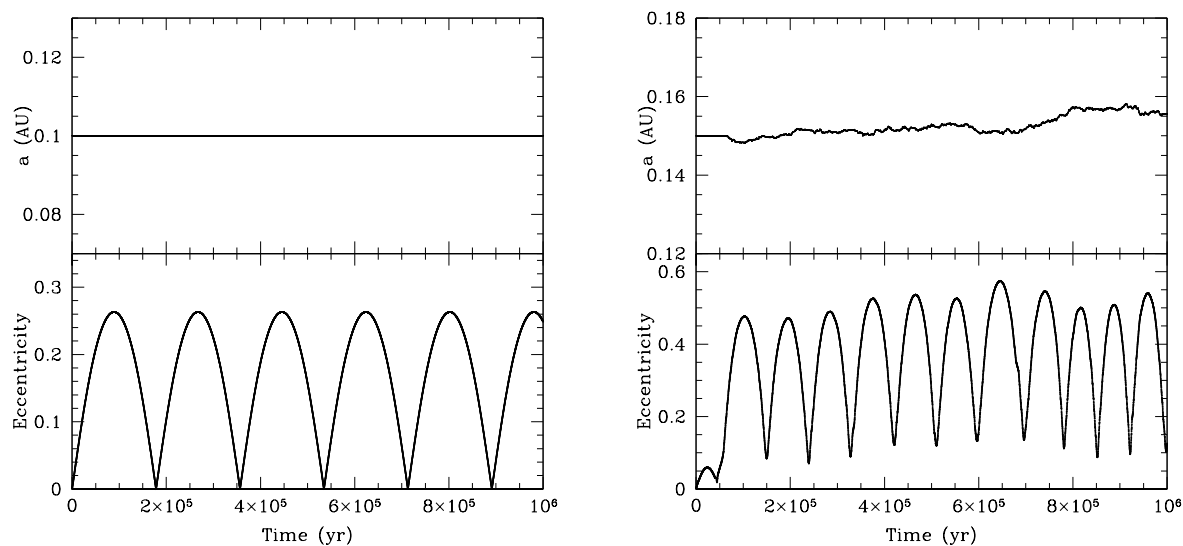


Fig. 16.— Left panel: Behaviour of the semimajor axis (top) and eccentricity (bottom) of a Saturn-mass test planet starting at  $a = 0.10$  AU in the HD 80606 system over a  $10^6$  yr period. Right panel: Same, but for an object starting at  $a = 0.15$  AU, which was then ejected at  $t = 5.7 \times 10^6$  yr.

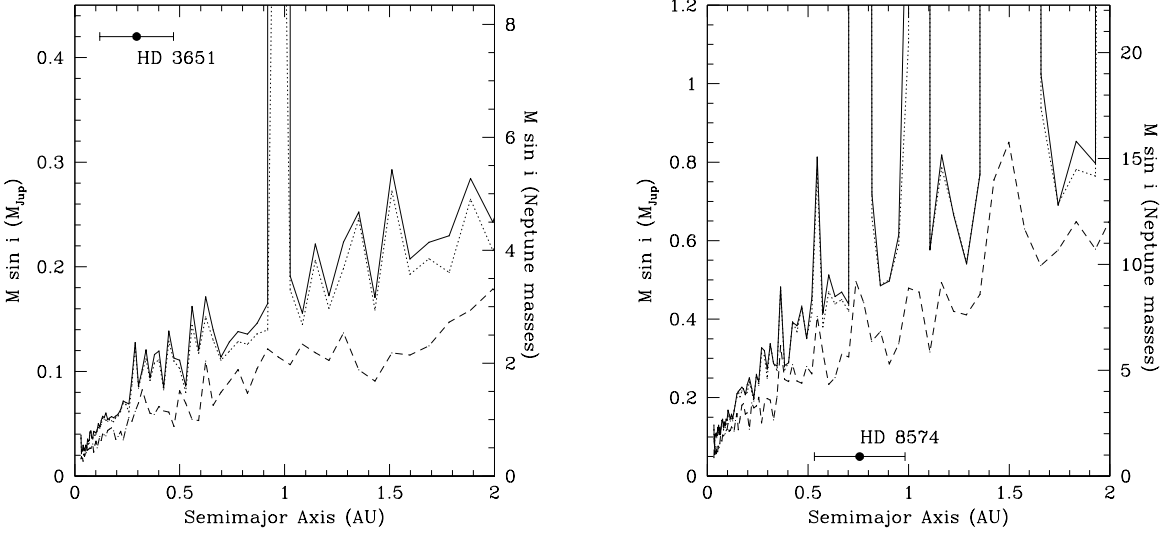


Fig. 17.— Left panel: Detection limits for additional planets in orbits with  $e = 0.20$  in the HD 3651 system (solid line). This value represents the mean eccentricity of surviving test particles from the dynamical simulations discussed in § 4. Planets in the parameter space above the solid line are excluded at the 99% confidence level. Limits for planets in circular orbits are shown as dotted (99% recovery) and dashed (50% recovery) lines. Right panel: Same, but for HD 8574 (solid line:  $e = 0.10$ ).

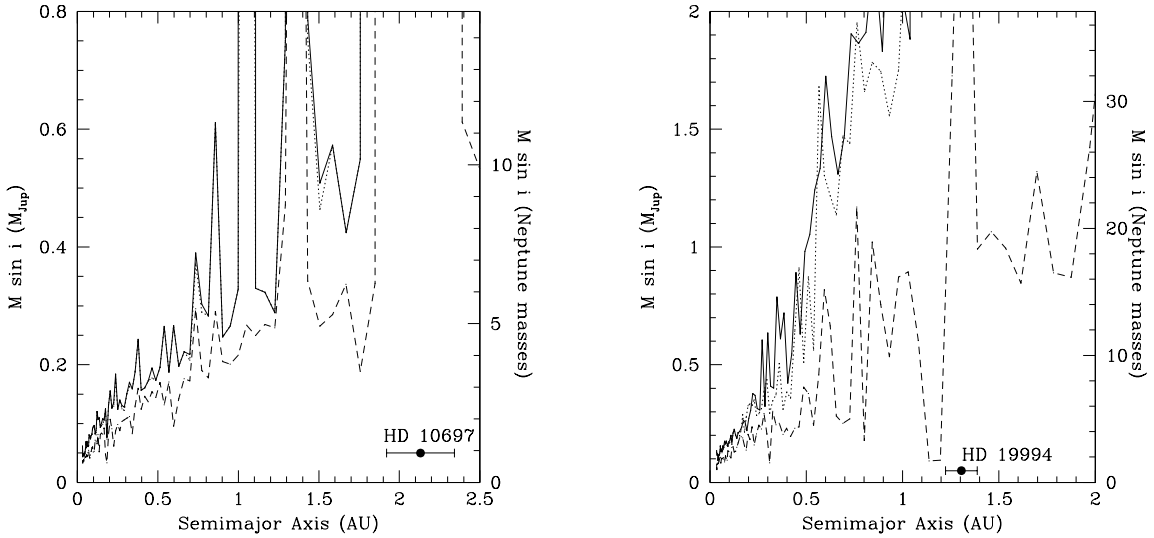


Fig. 18.— Left panel: Same as Fig. 17, but for HD 10697 (solid line:  $e = 0.04$ ). Right panel: HD 19994 (solid line:  $e = 0.09$ ).

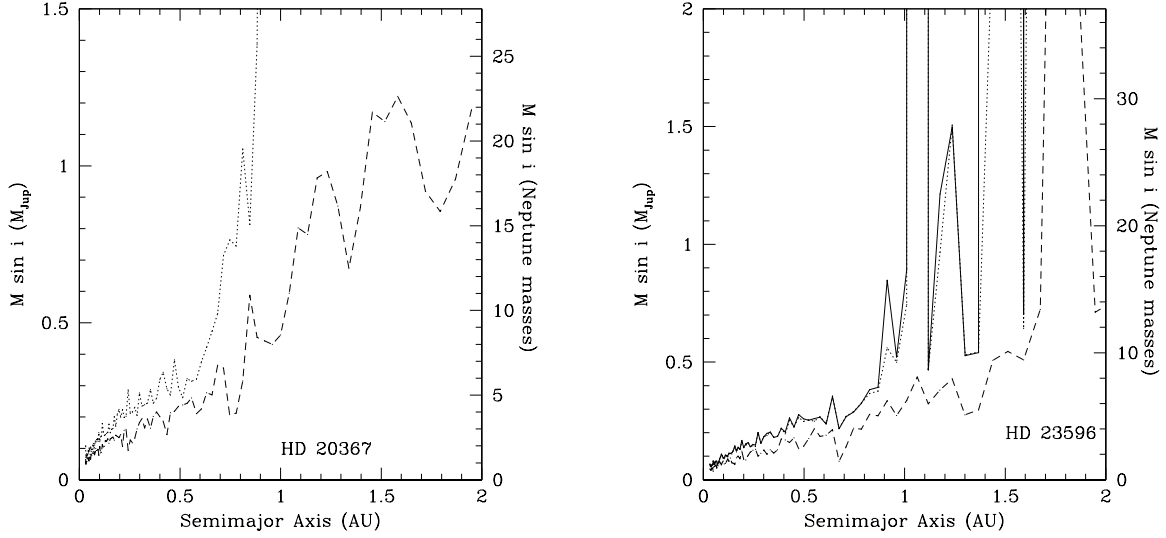


Fig. 19.— Left panel: Same as Fig. 17, but for HD 20367. These results were obtained without attempting to fit an existing planet, as no planet was confirmed in this system. Right panel: HD 23596 (solid line:  $e = 0.10$ ).

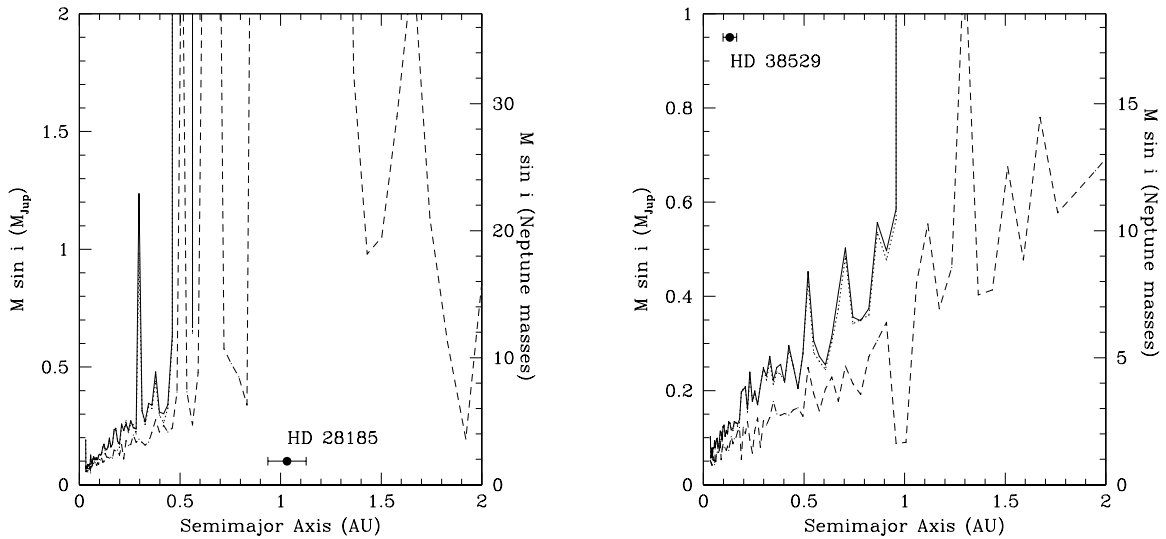


Fig. 20.— Left panel: Same as Fig. 17, but for HD 28185 (solid line:  $e = 0.09$ ). Right panel: HD 38529 (solid line:  $e = 0.12$ ).

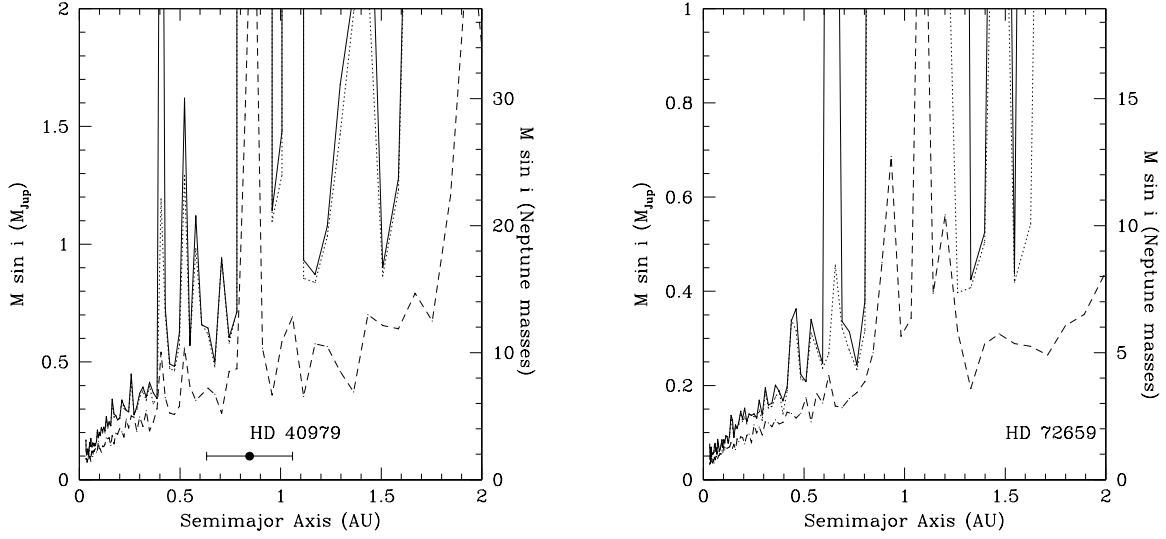


Fig. 21.— Left panel: Same as Fig. 17, but for HD 40979 (solid line:  $e = 0.11$ ). Right panel: HD 72659 (solid line:  $e = 0.10$ ).

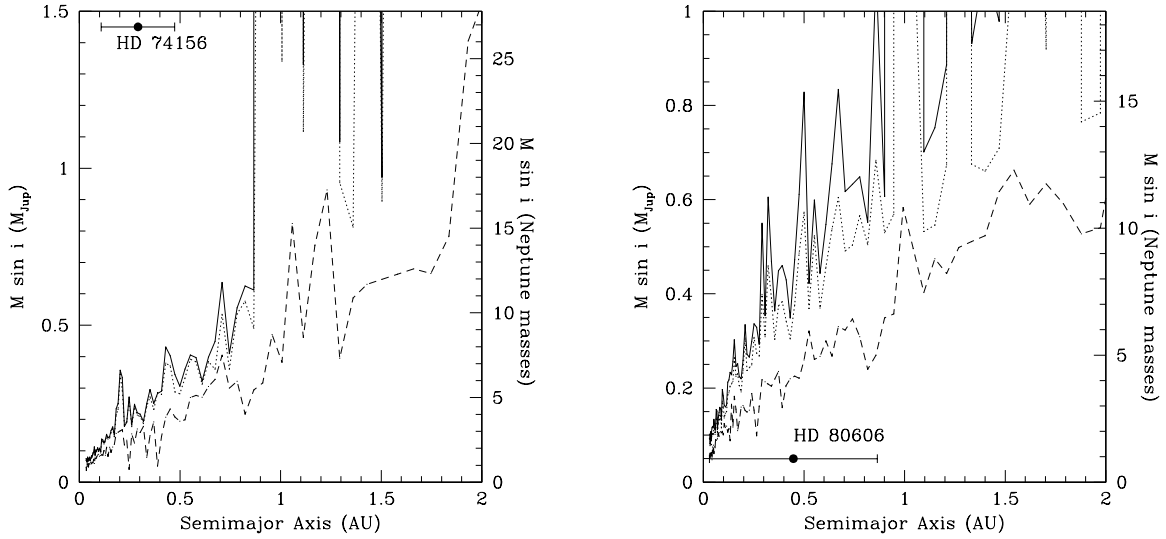


Fig. 22.— Left panel: Same as Fig. 17, but for HD 74156 (solid line:  $e = 0.15$ ). Right panel: HD 80606 (solid line:  $e = 0.31$ ).



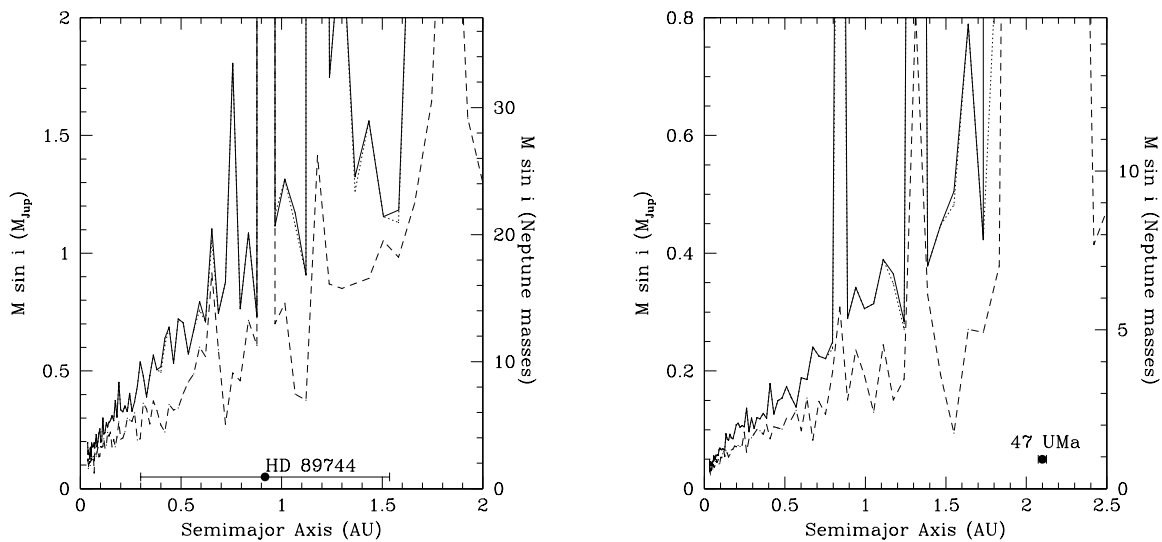


Fig. 23.— Left panel: Same as Fig. 17, but for HD 89744 (solid line:  $e = 0.01$ ). Right panel: 47 UMa (solid line:  $e = 0.02$ ). Only 47 UMa b was included in the limits computations.

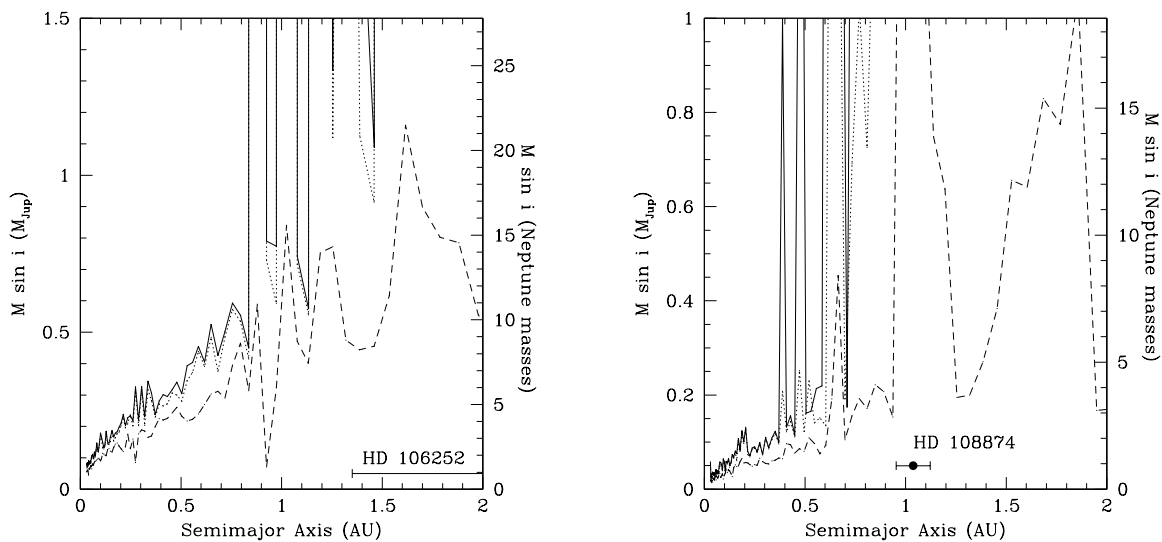


Fig. 24.— Left panel: Same as Fig. 17, but for HD 106252 (solid line:  $e = 0.15$ ). Right panel: HD 108874 (solid line:  $e = 0.15$ ).

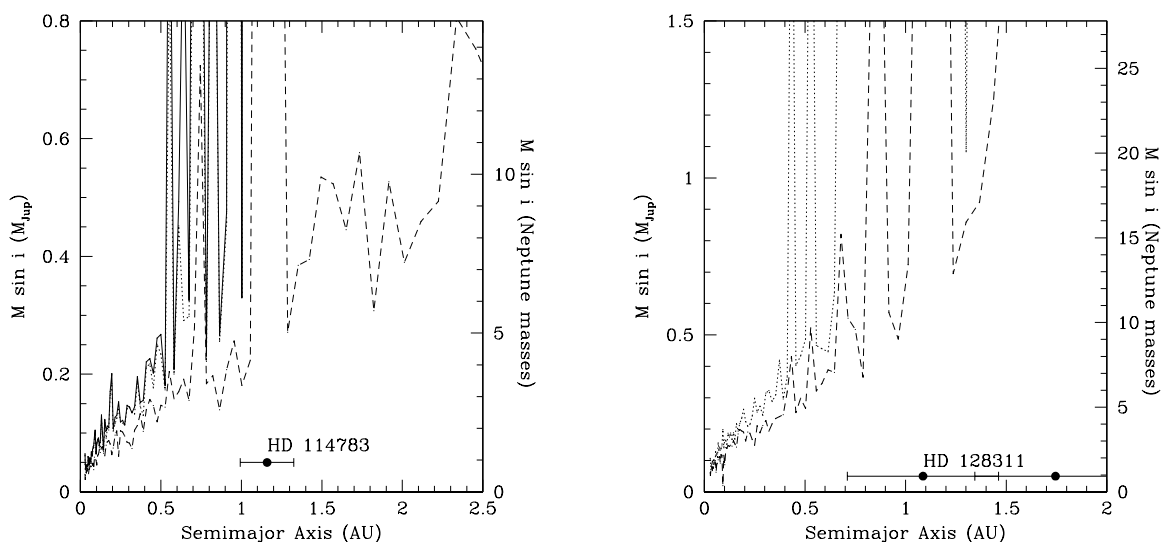


Fig. 25.— Left panel: Same as Fig. 17, but for HD 114783 (solid line:  $e = 0.11$ ). Right panel: HD 128311. Only circular orbits are considered since no test-particle simulations were conducted for this system.

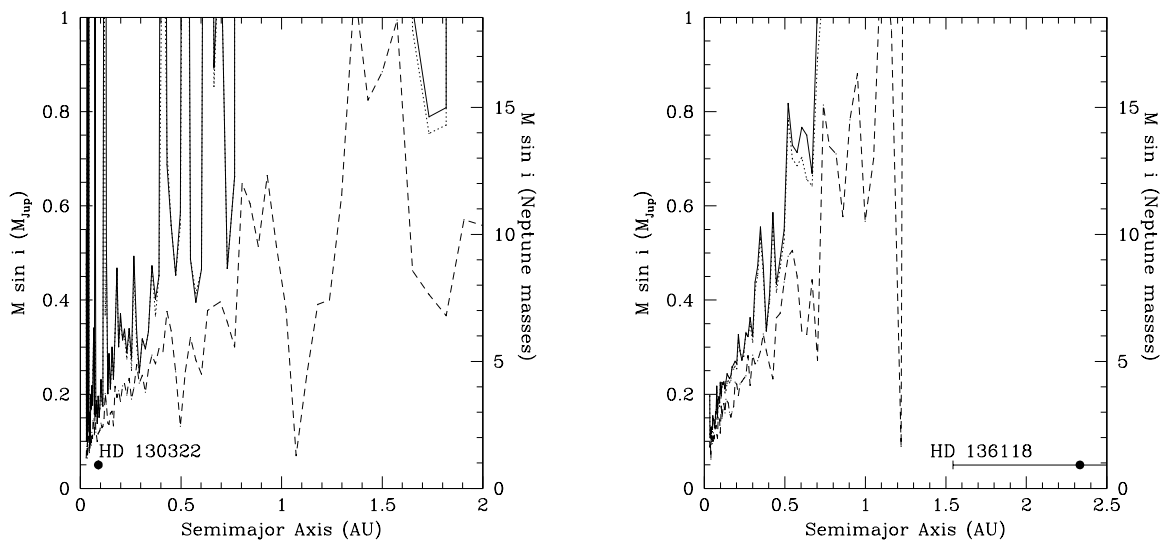


Fig. 26.— Left panel: Same as Fig. 17, but for HD 130322 (solid line:  $e = 0.02$ ). These results do not include data from Udry et al. (2000). Right panel: HD 136118 (solid line:  $e = 0.11$ ).

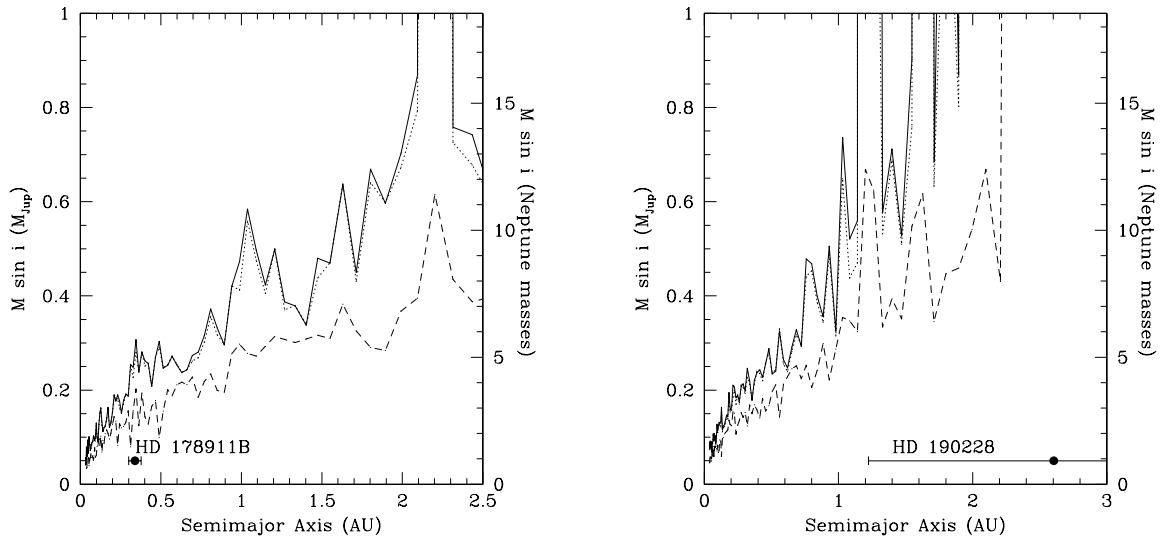


Fig. 27.— Left panel: Same as Fig. 17, but for HD 178911B (solid line:  $e = 0.07$ ). Right panel: HD 190228 (solid line:  $e = 0.16$ ).

Table 10. HET Radial Velocities for HD 3651

JD-2400000	Velocity (m s <sup>-1</sup> )	Uncertainty (m s <sup>-1</sup> )
53581.21162	14.4	3.7
53600.79860	0.4	4.7
53604.79357	-6.7	3.5
53606.78360	-9.3	3.9
53608.77426	-10.9	3.6
53615.96471	-18.5	3.6
53628.74240	3.8	3.3
53669.61203	-12.2	3.6
53678.79142	-10.0	3.6
53682.78611	-18.1	3.3
53687.77875	17.0	3.7
53691.76158	12.3	3.9
53694.75466	16.7	3.7
53696.76029	15.5	3.4
53955.83593	12.3	3.8
53956.83044	7.3	3.9
53957.82392	10.6	3.5
53973.80980	-4.3	4.7
53976.78586	-13.2	3.4
53978.97197	-2.2	5.9
53985.95982	-15.2	4.4
53987.95527	-13.6	3.0
53989.74009	-20.6	2.8
54003.70817	13.2	4.4
54005.68492	17.2	3.6
54056.78111	-9.9	3.5
54062.55312	19.0	3.4
54064.54902	13.0	3.3
54130.55508	15.4	3.4
54282.92879	-1.7	4.4
54352.96182	-9.8	3.1
54394.64607	-1.9	3.8
54399.61380	-9.2	3.5
54414.77832	-1.0	3.6
54423.75714	-14.9	4.4

Table 11. 2.7m Radial Velocities for HD 3651

JD-2400000	Velocity (m s <sup>-1</sup> )	Uncertainty (m s <sup>-1</sup> )
53633.86853	-3.3	5.0
53654.79777	6.6	6.6
53690.69920	-3.4	6.5
54020.84477	0.1	5.8

Table 12. HET Radial Velocities for HD 8574

JD-2400000	Velocity ( $\text{m s}^{-1}$ )	Uncertainty ( $\text{m s}^{-1}$ )
53601.81736	-40.9	6.3
53604.80314	-51.4	6.8
53605.82189	-42.2	6.9
53607.81271	-45.9	6.7
53609.79513	-48.9	7.3
53612.79858	-46.1	7.3
53633.96072	-30.7	7.8
53653.69022	-22.6	9.2
53663.88291	-27.5	9.0
53665.63807	-16.9	8.9
53668.64072	-25.3	8.7
53687.81363	-6.7	9.5
53695.79449	-2.5	11.0
53696.78211	6.2	10.6
53703.77271	34.9	9.6
53705.75396	37.0	9.8
53936.90653	38.7	7.5
53936.90653	42.1	11.1
53969.80550	61.9	7.4
53975.81126	64.7	10.6
53987.99307	55.7	9.0
53989.98424	66.3	9.6
53997.96536	29.8	8.1
54000.73798	18.7	10.0
54013.69475	4.2	8.7
54018.90830	-2.5	7.8
54043.84966	-31.4	10.2
54049.61516	-43.5	9.9
54057.78673	-38.9	9.9
54067.55166	-37.1	8.9
54071.76076	-50.1	9.7
54106.65631	-14.8	9.7
54110.66352	-12.7	10.5
54121.63331	-3.8	9.3
54306.89112	-30.4	8.2
54327.84854	-31.8	7.3
54344.80292	-26.1	7.9
54352.76329	-24.5	9.3
54367.73942	0.4	8.2
54402.85369	49.0	8.9
54402.86084	42.4	8.1
54404.84838	52.9	8.8
54419.81583	65.1	10.8
54434.54809	85.3	9.3



Table 13. 2.7m Radial Velocities for HD 8574

JD-2400000	Velocity ( $\text{m s}^{-1}$ )	Uncertainty ( $\text{m s}^{-1}$ )
52116.95398	24.0	9.6
52141.96262	70.0	8.0
52219.89758	-10.8	10.0
52249.70181	-30.2	9.6
52331.61330	1.7	7.7
52493.90858	-17.4	9.7
52540.91557	-13.9	8.9
52658.62787	-18.5	9.3
52932.83883	-45.8	8.9
53015.71309	29.6	9.2
53564.94976	2.1	10.8
53632.92472	-62.8	8.6
53635.90969	-22.1	8.4
53691.75684	-4.6	10.4
53970.92894	95.0	13.5
54018.87142	3.7	9.9

Table 14. HET Radial Velocities for HD 10697

JD-2400000	Velocity ( $\text{m s}^{-1}$ )	Uncertainty ( $\text{m s}^{-1}$ )
53581.90281	22.3	9.3
53606.84709	-21.0	8.7
53653.91334	-49.4	7.9
53663.69183	-43.8	8.9
53665.67577	-51.5	8.4
53681.83488	-67.6	8.4
53681.83752	-67.4	8.6
53690.81667	-60.4	10.3
53694.60078	-77.7	10.0
53696.79921	-73.3	9.2
53701.77012	-82.7	10.4
53703.79160	-70.7	10.0
53923.95145	-65.8	8.3
53954.87796	-47.2	8.5
53956.86965	-47.3	8.8
53958.88031	-46.6	9.0
53969.83080	-69.9	9.4
53971.83685	-61.7	8.8
53984.79870	-34.4	8.3
53988.80905	-26.3	8.5
53990.98655	-37.3	9.1
53999.74552	-28.7	7.8
54041.64127	-10.3	8.3
54042.65929	-10.5	8.4
54049.62382	-19.4	8.7
54056.63399	-3.7	10.6
54069.56942	14.7	9.7
54071.57888	6.6	9.8
54105.67044	33.5	8.9
54108.67092	23.4	9.2
54130.60755	41.9	10.4
54135.60424	60.0	10.3
54330.86457	130.5	8.7
54344.80964	108.3	8.8
54346.79984	124.2	8.4
54352.78595	136.5	9.3
54357.77232	114.1	8.2
54366.75077	119.1	9.1
54419.83538	117.8	11.5
54424.59411	121.5	9.1



Table 15. 2.7m Radial Velocities for HD 10697

JD-2400000	Velocity (m s <sup>-1</sup> )	Uncertainty (m s <sup>-1</sup> )
51066.97570	76.4	6.0
51152.79209	108.3	6.3
51211.61496	98.3	6.5
51239.60083	105.0	12.8
51449.91000	-20.3	5.3
51503.72131	-69.6	10.7
51529.67754	-72.8	7.6
51558.57566	-97.3	6.7
51775.92530	-83.4	5.6
51811.88858	-86.5	6.8
51859.67414	-64.9	5.8
51917.68431	-19.2	7.0
51946.64764	3.0	7.5
51987.56487	10.3	8.8
52116.96710	84.9	6.7
52247.79070	109.6	5.9
52306.67720	101.0	5.7
52493.92186	3.3	6.2
52539.87531	-31.9	5.7
52577.87821	-63.3	6.2
52897.88453	-68.5	8.2
52932.87904	-69.5	6.8
53017.69801	4.1	6.5
53215.85694	99.7	15.3
53215.87160	89.8	6.7
53320.75657	129.6	10.1
53564.96191	3.4	8.1
53566.91539	16.1	6.8
53635.89769	-51.9	8.8
53690.71397	-94.3	7.5
53968.92927	-88.3	10.9
54018.85867	-61.1	6.9

Table 16. HET Radial Velocities for HD 19994

JD-2400000	Velocity ( $\text{m s}^{-1}$ )	Uncertainty ( $\text{m s}^{-1}$ )
53605.28626	-22.1	5.1
53608.94050	-39.5	6.4
53612.92809	-26.6	6.2
53627.89670	-21.8	6.0
53633.88721	-3.1	6.7
53655.82407	11.6	6.3
53663.80786	5.6	7.5
53665.80005	10.1	7.1
53669.87714	9.5	7.2
53675.84787	5.1	7.6
53680.83658	20.6	7.5
53685.73881	18.7	7.3
53689.81169	29.1	7.7
53691.72151	34.3	7.8
53694.72971	20.8	8.6
53696.79236	24.2	8.2
53701.77903	36.5	8.6
53703.78435	36.2	9.1
53743.59301	46.2	8.0
53749.65649	58.6	6.9
53771.60345	42.0	9.0
53964.96481	7.0	6.6
53966.95936	-8.4	6.2
53985.91398	-30.2	7.1
53987.90646	-35.7	7.7
53989.91975	-31.4	6.6
53996.96612	-18.2	7.5
53998.88994	-11.4	7.9
54000.87587	-28.4	8.1
54003.87611	-16.3	7.4
54008.85651	-16.0	7.3
54018.91598	-25.5	7.6
54047.74879	-10.0	8.5
54050.73465	-10.5	8.3
54055.73818	-25.0	7.8
54061.72068	-27.8	7.5
54065.69886	-10.8	8.4
54067.70983	-9.9	8.9
54069.67713	-11.2	9.0
54071.73275	-13.2	5.5
54084.64261	-0.1	8.3
54105.58129	23.5	8.4
54122.62277	15.8	14.8
54130.61594	22.3	8.4
54330.98292	20.4	5.3
54352.90449	-15.2	6.2

Table 16—Continued

JD-2400000	Velocity ( $\text{m s}^{-1}$ )	Uncertainty ( $\text{m s}^{-1}$ )
54362.88624	4.0	6.4
54374.94279	12.9	6.6
54391.80959	9.0	8.3
54396.88855	20.4	7.2
54400.87136	12.8	7.6
54402.77756	-20.6	7.6
54415.83289	5.2	9.1
54419.82914	-20.9	9.0
54425.79502	-35.2	8.4
54428.70304	-4.9	8.0

Table 17. 2.7m Radial Velocities for HD 19994

JD-2400000	Velocity ( $\text{m s}^{-1}$ )	Uncertainty ( $\text{m s}^{-1}$ )
53635.94301	-2.0	9.7
53655.86581	-33.6	18.0
53690.87053	34.6	8.0
53747.67357	52.8	10.1
54020.88376	-33.9	8.5
54310.93898	22.2	10.4
54346.88504	2.7	11.4
54377.85942	-19.8	9.6
54404.79890	-4.2	8.9
54404.80349	-9.8	10.1
54460.79143	14.2	12.5
54496.57966	-23.3	8.5

Table 18. HET Radial Velocities for HD 20367

JD-2400000	Velocity ( $\text{m s}^{-1}$ )	Uncertainty ( $\text{m s}^{-1}$ )
53581.93777	9.2	8.3
53592.91499	13.0	11.9
53594.92230	-4.3	11.7
53605.87357	-1.8	10.8
53607.87923	-3.5	10.3
53608.87356	15.5	10.5
53610.85696	7.5	10.8
53612.85169	-8.8	12.3
53633.80562	-26.8	10.2
53651.98714	-1.9	10.3
53653.98515	17.0	10.7
53669.94716	8.3	11.2
53678.93317	-12.8	11.1
53685.89649	-19.5	10.6
53691.88485	-5.1	13.9
53694.88484	0.6	11.8
53696.65570	-0.2	11.7
53701.64348	-13.6	11.1
53703.85780	-0.3	11.9
53705.84073	-6.1	12.9
53708.83918	8.6	13.9
53710.83018	4.5	13.2
53713.60088	-6.3	11.8
53723.55489	-25.1	13.6
53725.79729	-10.8	11.4
53727.78708	-17.0	11.6
53728.78908	-18.0	12.7
53730.56553	-9.7	12.1
53730.76908	-10.7	11.3
53748.73406	28.8	11.0
53749.72703	27.3	10.7
53753.71868	16.4	12.7
53758.70824	1.5	12.8
53942.95869	3.4	11.2
53950.94642	-6.3	10.3
53954.92367	17.5	11.4
53956.92541	9.3	11.4
53958.90103	22.5	11.7
53960.92107	18.4	12.1
53970.88116	17.9	12.9
53976.88935	9.2	10.9
53979.86788	5.7	12.9
53979.87194	-10.9	11.1
53984.84306	-14.4	10.8
53988.84641	3.2	10.1
53993.83336	19.4	11.3

Table 18—Continued

JD-2400000	Velocity (m s <sup>-1</sup> )	Uncertainty (m s <sup>-1</sup> )
53997.82573	2.4	10.6
54001.81135	17.8	11.2
54018.98649	10.1	10.9
54021.74583	14.2	10.7
54035.71684	2.0	11.7
54044.92010	23.4	12.0
54051.88912	-6.1	12.4
54055.66817	19.9	11.6
54059.65106	-4.1	11.2
54065.64421	3.9	11.4
54067.62898	5.9	12.2
54071.84088	6.1	11.9
54071.84376	-17.6	11.9
54073.83664	6.6	13.0
54075.60874	-5.5	13.5
54133.68540	6.4	12.2
54141.66291	-2.2	10.8
54147.65026	6.0	10.5
54153.61823	6.0	11.3
54167.59481	-4.0	13.4
54169.57969	-14.2	12.0
54174.58417	7.7	11.4
54321.93181	-4.2	10.7
54347.86995	-9.4	10.9
54379.00296	-8.7	11.1
54394.73290	-11.1	11.9
54397.72206	-16.9	11.3
54399.71250	-10.4	10.2
54403.94387	-17.0	10.0
54409.90594	-18.6	12.4
54419.90334	-8.0	13.7
54419.90600	10.2	15.3
54425.65734	-5.1	10.6
54427.64289	-13.2	12.3
54427.64594	-23.0	11.2

Table 19. 2.7m Radial Velocities for HD 20367

JD-2400000	Velocity ( $\text{m s}^{-1}$ )	Uncertainty ( $\text{m s}^{-1}$ )
53632.00290	2.7	7.4
53635.96984	-3.7	8.2
53691.80381	-6.8	7.9
53808.62780	-7.9	6.2
53967.90828	11.5	8.2
53968.90725	11.4	10.8
54018.98018	-2.3	6.3
54158.59352	-5.9	6.7
54189.59664	-2.8	7.4
54189.61001	-6.9	7.7
54190.61247	-13.3	7.9
54191.60150	-1.9	6.1
54192.60131	4.3	5.5
54345.84686	0.1	8.3
54377.85210	-14.5	6.6
54402.79239	-3.6	5.9
54460.80432	-5.7	10.3
54496.58943	23.7	7.6
54555.60469	21.5	6.7

Table 20. HET Radial Velocities for HD 23596

JD-2400000	Velocity ( $\text{m s}^{-1}$ )	Uncertainty ( $\text{m s}^{-1}$ )
53581.96329	99.1	8.3
53592.92364	102.1	8.2
53593.94151	109.0	8.1
53594.92991	103.8	8.0
53605.89024	93.1	9.1
53607.89908	94.0	8.1
53608.88232	96.9	8.8
53609.89877	105.4	8.7
53627.84647	86.5	8.5
53629.84901	86.3	8.6
53636.81718	80.3	10.1
53668.74440	76.8	10.0
53677.71324	83.5	9.6
53677.71785	89.4	9.8
53680.71210	82.4	8.9
53682.70333	87.3	9.5
53691.89176	66.0	12.4
53694.67217	71.3	11.8
53696.66233	81.6	11.1
53701.64835	77.7	11.7
53703.87816	68.2	12.6
53708.84886	75.0	11.6
53710.83928	64.3	12.1
53712.85135	52.1	13.9
53712.85591	60.7	13.1
53734.78649	59.8	10.9
53741.76529	76.2	10.7
53748.74395	78.2	11.5
53800.58922	49.1	10.4
53956.94364	-5.3	8.6
53958.92009	-6.5	9.3
53960.92699	-10.2	7.4
53969.92325	-13.5	13.9
53973.90239	-9.6	11.6
53976.89466	-14.1	9.0
54057.66123	-45.2	9.8
54059.65849	-42.6	9.6
54064.88448	-53.3	9.3
54066.88228	-46.0	9.8
54068.65155	-53.9	11.4
54071.64397	-52.7	10.7
54073.86583	-12.4	11.1
54084.59010	-42.6	11.3
54092.57210	-48.2	11.7
54094.56514	-49.1	12.3
54130.71379	-58.2	8.8

Table 20—Continued

JD-2400000	Velocity (m s <sup>-1</sup> )	Uncertainty (m s <sup>-1</sup> )
54136.69786	-52.2	11.0
54147.66241	-49.4	10.1
54156.63332	-65.8	10.7
54159.61613	-60.2	11.3
54328.92108	-98.8	9.0
54370.81150	-122.1	7.9
54392.99377	-128.6	7.9
54394.74004	-131.4	9.0
54400.73405	-124.0	8.9
54403.72902	-116.3	11.0
54411.92379	-111.3	9.6
54419.91222	-129.5	10.3
54419.91687	-126.1	11.0
54419.92185	-123.5	10.3
54425.66281	-114.9	9.1
54427.65183	-118.7	11.3
54427.65648	-120.0	9.9

Table 21. 2.7m Radial Velocities for HD 23596

JD-2400000	Velocity (m s <sup>-1</sup> )	Uncertainty (m s <sup>-1</sup> )
53636.88979	73.6	7.1
53692.83650	48.7	7.6
53787.66076	11.9	6.0
53808.63976	13.0	7.1
54020.93260	-51.4	8.2
54158.60541	-95.8	6.1



Table 22. HET Radial Velocities for HD 28185

JD-2400000	Velocity ( $\text{m s}^{-1}$ )	Uncertainty ( $\text{m s}^{-1}$ )
53653.92112	-42.3	5.8
53663.89377	-38.0	7.0
53692.82400	24.8	6.3
53695.80664	42.7	6.8
53697.80395	34.2	6.8
53701.79069	43.3	8.0
53996.97502	-70.8	7.1
53998.99146	-64.8	7.7
54044.85384	-32.7	8.1
54051.83487	-17.9	6.7
54053.83800	-9.3	7.7
54061.80571	14.6	7.0
54063.79720	8.1	6.4
54066.79838	17.8	7.3
54068.78387	12.2	6.6
54071.77898	25.8	6.6
54073.77510	23.2	6.5
54075.76724	34.4	7.9
54105.68544	113.2	7.0
54107.68662	115.1	7.7
54110.67889	119.3	7.1
54142.58869	209.6	6.7
54368.95856	-53.6	6.8
54370.96073	-49.5	6.8
54374.94882	-50.1	6.8
54376.93838	-59.9	7.0
54390.90631	-43.2	6.1
54396.89578	-66.0	5.8
54400.87895	-53.6	6.7
54402.86922	-53.2	6.4
54404.86864	-44.3	6.3
54418.82544	-38.2	7.3
54425.80631	-38.5	12.6
54433.79452	-12.4	7.3

Table 23. HET Radial Velocities for HD 38529

JD-2400000	Velocity (m s <sup>-1</sup> )	Uncertainty (m s <sup>-1</sup> )
53341.50743	-186.9	3.2
53355.84573	-167.2	5.3
53357.85963	-181.3	5.4
53358.72474	-157.0	5.1
53359.72919	-144.0	5.9
53360.84952	-127.9	5.4
53365.81675	-82.4	4.6
53367.81264	-88.1	5.3
53369.70068	-158.4	5.4
53371.68476	-175.6	5.3
53377.78647	-92.2	6.2
53379.67580	-65.7	4.6
53389.75562	-101.2	4.9
53390.76324	-97.8	4.7
53391.75787	-88.0	5.1
53392.75205	-75.9	5.1
53395.73942	-57.5	4.8
53414.69383	-159.4	7.0
53416.68363	-136.9	5.4
53708.89443	2.7	4.8
53709.88697	-4.3	4.5
53711.76759	-45.3	4.2
53712.87586	-96.8	5.6
53724.84134	-4.7	4.5
53730.71767	-93.4	4.9
53731.70874	-77.7	4.7
53733.70635	-48.8	4.7
53735.71387	-20.3	5.0
53739.69217	-16.9	4.5
53742.68570	-107.9	4.4
53751.77576	24.2	4.8
53752.76272	22.8	4.7
53753.77304	11.6	5.2
53754.76015	-20.3	4.8
53755.75133	-61.2	4.5
53757.63903	-91.8	4.3
53758.75575	-87.3	5.5
53764.74541	6.2	4.4
53989.99899	21.1	4.5
54020.92423	81.0	4.0
54021.92187	95.7	4.3
54022.92612	101.0	7.9
54028.90307	28.2	4.4
54031.92844	55.3	3.4
54035.00746	105.3	4.1
54035.88704	111.6	4.8

Table 23—Continued

JD-2400000	Velocity (m s <sup>-1</sup> )	Uncertainty (m s <sup>-1</sup> )
54037.87620	126.6	4.2
54039.86912	117.0	4.5
54040.97263	85.6	4.3
54043.85975	32.4	4.4
54048.89153	96.4	3.4
54051.84308	120.3	4.5
54052.83905	132.7	4.5
54053.84658	132.0	4.7
54054.82922	112.6	7.2
54056.92288	33.4	4.8
54060.91436	53.1	4.7
54061.91194	70.9	4.6
54062.80705	85.5	4.4
54063.80866	102.5	4.2
54071.89032	37.3	4.1
54072.77450	34.0	4.4
54073.89412	32.3	4.5
54075.75720	70.5	3.9
54081.86774	169.9	4.8
54100.83215	43.0	5.5
54105.80466	122.6	4.7
54109.80132	170.3	4.8
54110.69101	162.4	4.7
54128.72971	71.1	4.6
54132.72555	101.9	6.5
54133.71881	112.2	4.3
54163.63702	153.6	4.7

Table 24. 2.7m Radial Velocities for HD 38529

JD-2400000	Velocity (m s <sup>-1</sup> )	Uncertainty (m s <sup>-1</sup> )
53633.96726	-44.5	5.7
53636.91593	-19.0	4.9
53691.91356	-24.9	5.8
53746.78728	-51.1	5.7
53809.64793	47.7	5.5
53984.94973	-1.4	5.1
54020.90382	93.2	6.4

Table 25. HET Radial Velocities for HD 40979

JD-2400000	Velocity ( $\text{m s}^{-1}$ )	Uncertainty ( $\text{m s}^{-1}$ )
53341.72130	-80.8	13.1
53346.73432	-99.4	15.1
53348.70934	-57.5	17.1
53350.72298	-81.2	14.7
53352.92178	-95.5	15.0
53355.68899	-48.4	13.4
53357.93997	-59.4	16.1
53359.68105	-88.5	16.3
53365.67253	-38.1	14.9
53367.66116	-10.1	15.9
53370.62842	11.0	16.9
53372.64584	55.1	42.5
53377.85739	20.0	23.3
53379.86066	48.2	15.6
53381.63007	69.2	13.3
53383.84999	77.1	14.6
53389.59831	67.5	15.8
53391.57735	84.0	16.8
53395.58085	117.5	13.1
53399.80045	104.5	12.1
53401.80944	131.8	13.1
53416.73452	97.1	13.1
53422.72494	105.6	11.1
53424.74945	71.9	12.6
53429.74027	89.5	11.6
53444.68952	91.8	13.9
53615.96771	-46.1	13.0
53623.94032	-20.7	13.6
53628.94576	-22.1	12.8
53629.92910	2.9	11.3
53633.91493	15.2	12.5
53638.90545	11.3	11.7
53646.89729	29.0	28.8
53651.88585	71.1	11.3
53655.87437	70.8	11.7
53663.84616	91.7	12.3
53666.83032	115.4	13.2
53668.81351	122.5	13.4
53669.82586	88.2	11.9
53676.82778	98.7	16.4
53678.79984	84.0	13.5
53681.80384	106.4	13.7
53683.80383	94.1	14.3
53685.79896	108.1	12.9
53687.78847	61.6	13.0
53689.78041	95.5	13.6

Table 25—Continued

JD-2400000	Velocity (m s <sup>-1</sup> )	Uncertainty (m s <sup>-1</sup> )
53691.77056	98.2	12.4
53693.99549	59.6	12.4
53696.97730	80.3	11.9
53701.75161	26.3	12.3
53703.96738	60.3	13.4
53705.96824	31.7	14.7
53708.94157	10.9	14.1
53710.94020	1.8	12.3
53713.94615	35.2	14.1
53713.94937	30.9	12.6
53721.90230	-23.6	15.9
53723.90854	3.6	12.7
53728.67332	-12.5	14.8
53730.65950	-18.9	14.1
53734.65127	-9.3	13.7
53743.62390	-1.6	17.0
53748.60983	-11.3	12.4
53753.84141	-54.3	12.7
53799.71352	-93.5	13.7
53801.70827	-96.0	11.9
53987.95684	-7.1	14.3
54014.89116	-75.8	12.4
54021.86435	-72.7	13.0
54037.82927	-99.6	14.2
54044.80399	-137.4	14.1
54053.00792	-124.9	11.7
54054.99336	-103.5	13.0
54057.99292	-114.8	11.9
54061.01007	-100.4	11.8
54068.73628	-120.0	13.4
54076.71914	-122.6	14.2
54101.86096	-147.8	15.7
54129.79577	-108.9	13.2
54132.78782	-94.0	14.4
54134.78060	-90.7	12.7
54136.76258	-89.7	12.9
54155.73508	-29.7	13.4
54166.70337	-0.7	12.3
54177.65752	39.5	12.8
54190.62821	119.0	11.9
54370.91031	-128.8	13.0
54397.83722	-83.0	11.5
54402.82966	-77.0	11.4
54414.00568	-71.8	13.1
54419.02519	-36.0	12.0



Table 26. 2.7m Radial Velocities for HD 40979

JD-2400000	Velocity ( $\text{m s}^{-1}$ )	Uncertainty ( $\text{m s}^{-1}$ )
53636.00527	78.9	8.9
53787.77595	-46.2	8.3
53864.61096	-23.4	7.6
54020.94453	-9.2	6.7

Table 27. HET Radial Velocities for HD 72659

JD-2400000	Velocity ( $\text{m s}^{-1}$ )	Uncertainty ( $\text{m s}^{-1}$ )
53342.98059	8.4	11.7
53346.89816	19.2	10.5
53348.89792	17.7	11.3
53351.88711	20.4	9.6
53355.85531	21.5	9.2
53357.86778	15.6	9.7
53359.86322	12.3	11.8
53366.92023	1.9	12.2
53370.82512	3.3	10.6
53375.89102	35.3	13.6
53377.89403	11.8	10.2
53379.88562	16.6	10.7
53383.88589	10.5	9.5
53389.78303	25.1	12.8
53391.78123	21.5	10.4
53395.75846	16.3	10.9
53399.83667	10.1	10.3
53401.82272	3.1	9.3
53408.71984	21.5	9.7
53416.69679	20.8	9.5
53422.69865	3.1	8.3
53424.76127	17.1	9.4
53429.75413	19.1	9.3
53439.64548	10.2	8.7
53446.69267	20.1	8.3
53447.69980	2.7	8.3
53448.70841	4.4	8.0
53708.90029	3.7	9.0
53710.89277	-4.4	8.8
53713.96630	2.2	10.0
53723.86387	2.1	8.8
53728.92778	-15.9	9.2
53734.90001	-15.7	11.2
53742.80266	-16.7	10.6
53746.79841	2.7	9.6
53751.79314	-10.5	10.3
53753.79398	-4.9	10.4
53755.85771	-8.2	10.6
53764.75640	-9.2	9.7
53773.72893	6.3	11.0
53780.78984	-1.5	9.4
53802.64977	6.8	8.3
54050.97483	-25.6	9.5
54053.02653	-18.5	9.5
54056.95675	-32.3	9.9
54061.02215	-29.7	9.6



Table 27—Continued

JD-2400000	Velocity (m s <sup>-1</sup> )	Uncertainty (m s <sup>-1</sup> )
54064.00548	-22.3	10.3
54127.75916	-29.3	8.4
54158.75638	-31.1	8.1
54161.66311	-21.2	9.8
54167.72203	-25.1	8.6
54420.02055	-50.6	11.1
54431.99247	-40.2	9.4

Table 28. HET Radial Velocities for HD 74156

JD-2400000	Velocity ( $\text{m s}^{-1}$ )	Uncertainty ( $\text{m s}^{-1}$ )
53342.23249	-119.8	7.9
53347.00129	-102.6	7.5
53355.83378	-93.1	7.9
53357.84523	-90.2	8.0
53359.85043	-79.3	10.8
53360.97444	-97.9	9.0
53364.97638	-99.2	10.4
53365.82597	-121.7	7.8
53367.82107	-127.5	8.8
53383.92077	-128.5	8.5
53390.75248	-107.2	8.0
53448.73888	-19.3	6.7
53451.73096	-31.0	7.2
53476.64913	-151.4	7.7
53480.63719	-167.2	22.9
53481.63192	-127.9	7.4
53482.63133	-96.2	7.5
53664.99582	75.5	7.0
53675.97107	61.4	7.8
53676.98443	53.1	8.9
53682.95189	-46.4	8.3
53687.93153	-54.2	7.3
53689.92922	-1.3	7.5
53691.91679	27.3	7.9
53697.91227	50.3	7.7
53703.88616	71.2	9.3
53708.88180	81.0	8.6
53710.87934	81.4	7.7
53718.01348	62.8	10.1
53724.82993	70.8	8.2
53728.82485	47.9	7.9
53731.96775	16.0	9.3
53733.80186	-33.8	9.2
53734.80949	-58.8	8.6
53736.94379	-138.8	9.2
53741.78326	3.4	8.5
53742.78352	10.0	8.1
53743.79031	33.9	8.3
53748.77268	67.4	8.7
53751.76772	84.5	8.8
53753.76343	99.6	8.3
53754.74931	90.1	7.9
53756.74864	92.3	8.3
53764.73571	90.9	9.3
53832.67552	50.9	7.2
53833.69639	52.0	8.1

Table 28—Continued

JD-2400000	Velocity (m s <sup>-1</sup> )	Uncertainty (m s <sup>-1</sup> )
53834.67429	33.9	7.5
53835.66675	12.8	7.4
53838.66377	-82.9	7.3
53841.64454	-93.6	11.0
53845.63199	17.1	7.7
53846.65288	34.0	7.7
54029.98957	56.8	7.6
54035.99026	47.8	8.2
54038.97806	37.1	7.5
54039.97014	30.0	7.6
54040.95851	18.0	7.7
54043.96476	-43.3	6.8
54044.95388	-92.8	6.7
54050.95326	-35.4	7.7
54051.94621	-16.1	8.4
54052.93930	1.4	7.0
54073.88022	56.5	6.8
54079.86417	63.8	7.2
54087.84388	53.6	6.8
54090.83839	28.0	7.0
54106.78411	9.3	8.6
54109.78878	20.6	7.1
54110.79989	26.4	8.3
54129.87053	51.6	8.8
54130.74036	48.8	8.6
54133.84698	36.1	8.9
54134.72603	46.7	8.9
54135.86669	43.7	8.5
54136.84113	43.9	9.7
54148.67767	-128.1	10.6
54156.66058	-1.7	9.3
54159.77984	24.0	8.8
54166.76336	45.8	7.9
54167.75867	40.7	8.1
54211.63030	7.8	7.9
54231.60002	58.8	6.4

Table 29. HET Radial Velocities for HD 80606

JD-2400000	Velocity (m s <sup>-1</sup> )	Uncertainty (m s <sup>-1</sup> )
53346.88103	8.1	8.6
53358.02089	-16.0	8.1
53359.82400	-26.7	8.8
53361.02985	-28.9	7.7
53365.03079	-46.8	8.0
53373.98282	-63.3	9.8
53377.80112	-62.8	9.6
53379.75230	-62.1	9.3
53389.74170	-95.6	7.8
53391.74400	-97.6	8.0
53395.72763	-104.1	8.6
53399.72518	-115.4	9.4
53401.72497	-123.7	9.1
53414.67819	-186.7	9.1
53421.85529	314.1	8.1
53423.86650	374.2	7.9
53424.85231	302.6	7.3
53432.87120	132.0	7.6
53433.60628	119.8	7.6
53446.79322	55.8	8.2
54161.85400	-62.4	8.9
54166.83797	-80.2	7.3
54186.76189	-134.1	7.4

Table 30. HET Radial Velocities for HD 89744

JD-2400000	Velocity (m s <sup>-1</sup> )	Uncertainty (m s <sup>-1</sup> )
53709.89685	93.4	11.8
53723.85367	57.9	8.7
53727.84573	70.0	9.0
53734.81973	64.1	9.1
53736.82101	60.8	9.9
53738.03441	76.6	9.8
53738.81040	76.7	9.6
53742.79299	66.5	9.0
53746.81778	51.1	8.7
53751.78379	53.7	10.7
53753.78381	45.4	8.7
53755.76218	47.2	9.2
53757.77181	35.1	9.1
53797.64834	-165.1	10.0
53809.62700	-353.0	8.7
53837.77709	1.2	7.9
53866.70329	97.6	7.5
53868.68562	100.3	13.0
53875.66956	102.4	11.6
53883.65837	114.7	6.5
53890.63954	107.9	7.1
53893.63138	125.0	7.2
54050.96453	-137.3	7.5
54052.96762	-160.3	6.9
54056.94785	-197.9	7.6
54063.93165	-327.2	7.9
54073.91476	-438.1	9.1
54122.01243	102.1	9.5
54129.74491	94.8	10.1
54160.66031	98.0	9.6
54163.66643	89.0	10.0
54165.88148	98.8	15.3
54421.94999	75.7	8.1

Table 31. 2.7m Radial Velocities for HD 89744

JD-2400000	Velocity (m s <sup>-1</sup> )	Uncertainty (m s <sup>-1</sup> )
53690.03080	262.2	7.7
53805.87856	-129.3	7.1
53806.73923	-130.0	8.9
53807.83562	-188.4	10.8
53809.79691	-198.1	7.8
53840.78664	168.0	9.8
53864.76543	203.8	8.9
53911.61226	252.5	9.3
54068.94214	-240.7	8.7

Table 32. HET Radial Velocities for 47 UMa

JD-2400000	Velocity (m s <sup>-1</sup> )	Uncertainty (m s <sup>-1</sup> )
53313.33003	24.4	4.7
53314.99108	31.8	4.6
53317.99083	30.8	4.4
53334.95254	26.0	4.3
53335.94709	26.8	4.4
53338.93789	20.1	3.1
53340.91724	24.8	4.4
53346.92207	17.7	4.3
53348.90940	24.0	4.7
53350.91700	14.7	8.2
53357.88009	4.3	5.0
53359.87543	7.9	5.6
53365.86490	-11.9	4.1
53367.86390	1.0	4.3
53371.85734	-1.0	5.1
53373.85855	1.0	7.9
53377.83382	3.4	4.4
53379.85077	-4.9	4.5
53389.79762	4.0	4.2
53391.79286	-6.9	5.0
53395.77820	-4.5	4.4
53400.99471	-3.3	4.7
53408.76968	-1.7	4.5
53414.72833	-10.6	4.3
53416.71040	-9.0	4.7
53421.94116	-7.1	3.8
53423.70482	-13.1	3.5
53429.91553	-7.8	3.2
53432.90803	-5.9	3.3
53433.90682	-7.8	3.2
53437.66207	-6.9	2.8
53439.65955	-7.0	3.2
53440.90030	-13.2	3.7
53476.80401	-20.0	3.3
53479.77845	-16.3	3.2
53481.76620	-16.9	3.3
53486.77731	-20.7	3.4
53488.76788	-20.1	3.2
53512.69186	-12.1	3.3
53526.63730	-15.7	2.6
53539.63923	-14.5	3.6
53708.92005	-27.1	4.8
53709.92253	-29.2	4.7
53710.91317	-29.6	4.2
53711.93277	-26.4	3.6

Table 32—Continued

JD-2400000	Velocity (m s <sup>-1</sup> )	Uncertainty (m s <sup>-1</sup> )
53721.88029	-19.6	4.9
53723.87033	-29.2	4.8
53725.86147	-21.3	4.8
53734.87812	-39.1	4.9
53736.84137	-30.0	4.7
53738.82751	-24.4	4.5
53742.82008	-31.4	4.7
53743.82024	-36.6	5.4
53744.82292	-26.8	4.4
53746.80758	-23.2	4.5
53751.79987	-26.4	5.0
53757.03749	-29.7	4.2
53771.76109	-18.3	4.8
53775.74040	-16.1	4.1
53777.96664	-16.3	4.6
53779.96405	-21.1	4.3
53786.70738	-16.1	5.0
53795.91970	-17.0	3.0
53797.66773	-5.6	5.4
53894.65514	18.2	3.6
53901.64093	21.6	3.8
54050.99305	53.7	4.0
54052.99278	65.9	4.0
54054.97972	53.9	4.2
54056.96223	47.0	4.2
54121.81209	47.7	4.8
54129.77513	51.6	4.9
54157.70092	70.7	4.7
54160.68446	63.1	4.8
54165.91204	64.2	4.3
54419.99530	17.4	4.3
54431.94398	9.9	4.3

Table 33. 2.7m Radial Velocities for 47 UMa

JD-2400000	Velocity (m s <sup>-1</sup> )	Uncertainty (m s <sup>-1</sup> )
51010.62898	52.2	6.2
51212.97474	1.7	4.5
51240.81250	-1.7	4.6
51274.78993	-8.8	4.6
51326.70558	-24.5	4.9
51504.95996	-39.7	5.0
51530.01978	-27.0	5.1
51555.94972	-15.5	4.8
51655.74023	-0.7	4.7
51686.75156	-8.8	6.0
51750.60418	13.1	5.1
51861.01895	53.7	4.9
51917.93086	48.2	4.6
51987.85527	53.7	6.2
52004.83235	60.5	4.8
52039.77936	54.5	5.9
52116.60554	55.7	6.6
52249.00010	21.6	5.4
52303.89238	-8.3	5.1
52305.84757	-1.5	4.7
52327.86285	21.2	13.1
52353.85949	2.6	6.1
52661.95399	-30.8	4.7
53017.93695	75.2	6.4
53069.76686	54.9	4.2
53692.03243	-44.4	6.5
53748.89147	-40.4	4.6
53787.91198	-28.0	4.7
53805.88756	-28.3	4.5
53809.80777	-25.0	4.7
53840.77154	-19.2	5.1
53841.70627	-19.3	5.8
53841.72168	0.2	6.5
53861.74397	-19.8	5.4
53909.61977	3.6	5.7
54280.64401	38.2	6.7
54280.64893	31.4	5.6
54551.92162	-36.6	5.2
54569.78354	-39.5	5.8
54569.78813	-37.8	5.9
54569.79271	-40.3	6.1
54605.77977	-52.7	6.5
54632.71638	-43.6	6.9



Table 34. HET Radial Velocities for HD 106252

JD-2400000	Velocity (m s <sup>-1</sup> )	Uncertainty (m s <sup>-1</sup> )
53351.00010	-86.7	10.2
53392.87552	-19.4	11.1
53396.02801	-18.2	10.0
53399.86570	-0.6	11.5
53422.81038	35.5	8.9
53423.95949	38.5	9.9
53424.95405	30.2	8.4
53429.93417	43.4	8.3
53436.93141	41.8	8.3
53439.93691	44.2	9.3
53440.93473	46.8	10.0
53448.72404	54.7	8.7
53449.71116	60.8	9.4
53450.72302	50.1	8.7
53451.72210	49.4	8.3
53452.88054	66.6	8.6
53454.86997	56.3	8.8
53455.86893	64.1	8.8
53457.70319	60.4	8.6
53480.62813	72.9	10.0
53487.78674	69.1	9.0
53498.76669	82.5	9.9
53543.64221	92.8	8.7
53736.92178	-13.3	10.6
53736.92786	-9.9	9.9
53743.93096	1.6	11.4
53744.90904	-12.4	9.7
53745.89603	-11.5	9.8
53753.89366	-17.2	9.3
53755.88492	-24.8	9.0
53758.87460	-32.4	9.9
53765.02009	-25.5	11.8
53779.82267	-24.6	10.3
53796.76996	-34.1	8.4
53866.75798	-41.3	10.2
53868.73636	-39.5	9.5
53877.71039	-35.1	8.4
53891.67012	-40.6	8.4
54090.96158	-100.9	8.1
54110.90994	-106.5	8.8
54122.04519	-118.5	9.6
54161.76867	-124.4	9.8
54191.69138	-124.3	8.6

Table 35. 2.7m Radial Velocities for HD 106252

JD-2400000	Velocity ( $\text{m s}^{-1}$ )	Uncertainty ( $\text{m s}^{-1}$ )
52116.61921	46.4	11.5
52307.00335	16.9	9.8
52328.89167	-32.1	11.8
52357.80730	-40.7	9.6
52743.85538	-129.6	9.1
53465.74189	55.7	10.4
53504.65833	73.1	9.8
53564.63133	73.7	10.5
53566.62685	84.6	10.8
53808.85919	-23.7	10.3
53842.77638	-24.6	10.9
53861.78041	-35.8	10.2

Table 36. HET Radial Velocities for HD 108874

JD-2400000	Velocity (m s <sup>-1</sup> )	Uncertainty (m s <sup>-1</sup> )
53370.93479	-4.1	7.6
53377.90734	3.4	8.0
53392.86111	-3.8	8.3
53399.84978	4.9	7.1
53423.00572	1.5	6.0
53424.00026	-1.7	6.4
53429.76827	9.2	5.6
53446.93347	3.5	6.4
53449.92196	-0.3	5.6
53451.70786	4.7	5.5
53452.91476	-0.6	5.0
53454.90261	-10.7	6.1
53455.91231	-2.2	5.6
53457.89845	-9.3	5.8
53460.88699	-5.9	6.0
53708.98585	-35.6	7.5
53723.95560	-17.0	7.7
53730.92665	-15.4	7.5
53751.89671	-3.0	7.1
53753.88047	-3.1	7.8
53755.87205	9.2	6.3
53773.81280	11.5	6.7
53806.96496	3.7	6.8
53847.61993	5.4	6.1
53866.78797	-3.3	6.2
53868.77287	-6.4	5.8
53880.76028	-3.9	6.5
53895.71194	-5.6	5.3
53897.70685	-3.1	5.7
53912.66615	-12.8	5.3
54080.96833	-24.1	7.0
54084.96842	-25.8	7.1
54109.89738	-1.9	7.0
54127.85761	3.1	6.8
54142.02401	17.2	6.6
54158.76779	28.1	7.7
54160.75928	23.2	6.7
54162.75513	19.0	7.0
54180.92025	23.0	5.8
54190.88453	29.0	6.2

Table 37. HET Radial Velocities for HD 114783

JD-2400000	Velocity ( $\text{m s}^{-1}$ )	Uncertainty ( $\text{m s}^{-1}$ )
53366.02839	-17.8	6.0
53368.02525	-25.3	5.5
53374.00882	-13.9	6.5
53378.99750	-16.3	5.3
53395.95201	-23.9	5.4
53399.94906	-25.0	5.2
53415.90535	-27.0	6.2
53416.96080	-27.8	5.7
53421.88527	-21.5	5.5
53423.88025	-29.5	5.9
53429.88531	-19.4	5.7
53436.92048	-22.8	5.6
53440.91863	-24.7	6.9
53446.81643	-20.4	5.2
53447.81352	-16.1	5.5
53448.81555	-13.6	5.6
53450.81211	-18.4	5.5
53451.82012	-22.9	5.2
53452.81032	-16.8	5.5
53455.78717	-20.4	5.3
53779.91198	6.9	5.7
54097.02928	27.2	5.7
54106.00717	32.2	6.0
54121.96750	24.7	5.3
54127.95124	28.9	5.3
54130.94440	35.9	5.3
54140.98702	26.0	5.7
54143.92794	21.4	6.0
54156.87064	35.6	5.8
54158.87301	34.8	5.8
54163.85683	38.2	5.8
54168.83901	42.2	5.6
54186.78882	32.9	5.0
54191.77547	36.7	5.2

Table 38. HET Radial Velocities for HD 128311

JD-2400000	Velocity ( $\text{m s}^{-1}$ )	Uncertainty ( $\text{m s}^{-1}$ )
53462.96527	-137.0	4.1
53479.81567	-147.0	4.4
53480.91902	-136.9	5.7
53482.89103	-144.3	5.7
53486.72671	-159.9	5.5
53488.70965	-168.8	6.4
53509.81664	-160.8	6.0
53510.82254	-172.4	5.6
53511.80800	-176.2	6.0
53512.80394	-159.5	5.6
53539.74332	-177.2	4.7
53541.75663	-152.9	5.7
53542.74601	-159.5	5.3
53544.73511	-163.9	4.8
53550.71539	-162.3	5.8
53554.69916	-165.3	5.4
53565.69081	-159.0	6.1
53570.66963	-124.8	6.3
53776.92892	-55.4	6.3
53788.90110	-65.9	7.7
53816.97394	-81.9	6.2
53824.80309	-88.4	6.2
53837.91730	-115.2	5.9
53842.75039	-53.5	6.4
53844.91973	-87.7	5.7
53846.91450	-118.5	5.0
53888.79633	-92.8	5.1
53895.75921	-149.3	5.0
53897.76919	-106.0	4.8
53899.76175	-76.0	4.6
53911.71053	-80.0	5.4
53926.66439	-131.2	6.4
53933.66149	-56.4	4.9
54108.00385	1.0	4.4
54110.00828	9.5	3.7
54111.00546	-1.6	3.9
54130.96180	11.2	3.8
54133.93944	9.9	4.5
54135.94222	34.9	4.2
54138.92468	14.5	4.0
54139.92656	-4.1	4.0
54141.92573	21.5	3.7
54156.87834	49.1	4.5
54157.88752	62.4	5.0
54158.88100	47.6	4.5
54160.87801	21.5	4.5

Table 38—Continued

JD-2400000	Velocity (m s <sup>-1</sup> )	Uncertainty (m s <sup>-1</sup> )
54161.86725	19.6	4.0
54163.86833	41.8	3.9
54164.85995	54.8	6.2
54168.84642	70.2	6.2
54173.87121	31.0	3.2
54174.99073	50.0	5.2
54177.00300	62.6	3.5
54186.80132	42.8	3.5
54190.80340	69.2	3.6
54191.87047	70.0	3.7
54211.91614	59.3	4.0
54214.71537	69.1	4.1
54216.72250	41.2	3.5
54217.87848	31.4	3.7
54221.70097	59.8	3.5
54222.71695	58.2	3.3
54223.88092	64.8	3.6
54231.85098	64.0	3.4
54232.85136	53.4	3.2
54249.79485	41.0	3.5
54250.79070	39.8	3.2
54251.63068	19.8	3.3
54253.78617	46.3	3.1
54254.79359	39.2	3.2
54255.78044	33.1	3.5
54257.77841	50.0	3.2
54265.75347	22.7	3.2
54267.74859	31.4	3.5
54276.71906	0.8	3.6
54278.71354	3.1	3.2
54279.72454	11.9	2.7
54318.61493	-83.4	5.3

Table 39. HET Radial Velocities for HD 130322

JD-2400000	Velocity (m s <sup>-1</sup> )	Uncertainty (m s <sup>-1</sup> )
53471.80558	-99.8	7.2
53481.88526	-106.9	6.6
53486.85864	105.1	6.4
53488.75815	72.2	5.9
53509.79117	101.3	6.1
53512.78123	-65.6	5.1
53527.74971	27.0	6.2
53542.69985	55.4	5.6
53543.70614	-4.9	6.1
53550.70420	105.5	6.1
53837.89677	-12.6	5.9
53842.88880	27.6	6.3
53868.80896	-78.8	5.7
53882.78043	83.0	6.0
53897.72683	-44.2	6.1
53900.72079	-85.4	6.0
53936.63557	110.4	6.6
54122.01834	-12.7	6.8
54128.00335	47.0	6.7
54135.98084	-113.2	6.5
54139.97029	89.9	7.2
54140.96840	98.1	6.1
54144.96962	-99.4	6.6
54157.01611	-112.4	6.8
54158.92425	-40.9	6.8
54163.92465	26.3	6.7
54168.90656	-71.6	6.5
54173.98269	69.7	7.4
54176.87914	-90.6	5.7
54191.92631	20.5	6.2

Table 40. 2.7m Radial Velocities for HD 130322

JD-2400000	Velocity (m s <sup>-1</sup> )	Uncertainty (m s <sup>-1</sup> )
53585.64900	83.7	7.5
53843.89253	-18.0	7.5
53863.78301	75.5	8.6
53910.78043	-68.5	8.1
54251.84318	-72.8	9.4

Table 41. HET Radial Velocities for HD 136118

JD-2400000	Velocity (m s <sup>-1</sup> )	Uncertainty (m s <sup>-1</sup> )
53471.83434	37.0	7.8
53480.89983	11.8	11.6
53482.88067	8.1	9.0
53486.86878	12.1	14.7
53487.88314	17.0	9.0
53509.80853	15.5	12.8
53527.76309	5.7	9.4
53544.72664	4.5	9.3
53575.62972	1.1	9.4
53755.05078	-101.1	11.1
53757.04207	-101.7	10.1
53758.03539	-88.4	15.3
53766.02629	-101.5	9.7
53767.02021	-87.2	16.8
53769.01091	-95.3	8.8
53778.99248	-97.5	14.3
53779.98920	-103.4	15.6
53787.98168	-92.7	8.9
53803.01595	-97.6	13.2
53805.98952	-85.6	13.7
53808.90657	-92.2	7.6
53809.90878	-93.7	10.3
53815.88767	-71.7	8.2
53816.93136	-81.2	6.9
53818.87257	-73.7	9.2
53820.89349	-80.5	8.8
53832.83912	-83.6	9.2
53835.85292	-80.7	9.6
53836.85837	-73.5	13.4
53840.89490	-81.0	8.6
53842.89836	-75.4	14.4
53844.90864	-68.2	7.9
53866.77360	-63.9	8.0
53867.75385	-71.4	7.7
53868.75220	-62.9	11.9
53877.74161	-68.8	7.3
53880.80832	-87.9	8.9
53883.77783	-76.4	7.5
53888.69980	-75.5	8.0
53890.67902	-52.4	8.2
53891.68247	-58.2	7.8
53892.68903	-68.8	7.9
53893.76811	-76.9	7.5
53895.74381	-47.5	15.6
53897.74893	-69.6	7.5
53898.67744	-73.1	8.7



Table 41—Continued

JD-2400000	Velocity (m s <sup>-1</sup> )	Uncertainty (m s <sup>-1</sup> )
53901.74015	-66.1	8.3
53905.73368	-58.2	9.0
53911.73001	-42.9	8.7
53917.68891	-35.2	13.9
53937.64758	-71.9	12.8
53939.63048	-64.2	13.2
54129.03715	172.5	8.6
54131.02378	179.1	9.8
54144.99774	185.3	13.1
54164.01886	249.5	12.5
54176.99293	279.5	7.4
54180.88946	287.4	8.3
54186.88695	309.8	7.9
54190.87336	306.2	15.1
54211.81162	313.7	8.3
54221.78932	331.8	8.6
54253.69912	346.9	6.9
54282.63079	329.9	8.9

Table 42. 2.7m Radial Velocities for HD 136118

JD-2400000	Velocity (m s <sup>-1</sup> )	Uncertainty (m s <sup>-1</sup> )
53585.66699	13.5	11.4
53805.93741	-1.7	9.1
53863.76953	-12.0	13.8
53911.75165	0.2	10.0

Table 43. HET Radial Velocities for HD 178911B

JD-2400000	Velocity (m s <sup>-1</sup> )	Uncertainty (m s <sup>-1</sup> )
53653.66528	-57.4	6.2
53801.00302	-217.2	6.1
53803.02412	-268.6	6.2
53837.93570	257.0	6.7
53846.89693	323.3	5.6
53866.83649	-19.7	5.6
53868.81760	-86.7	6.2
53883.79325	-343.1	4.5
53954.82320	-349.3	5.7
53955.82606	-336.2	5.4
53956.82027	-326.8	5.8
53958.81704	-291.4	5.5
53960.80356	-245.8	5.5
53965.80165	-102.8	5.4
53966.78694	-69.2	5.3
53971.77135	72.4	5.6
53976.76788	181.7	5.7
53979.76859	242.2	6.0
53988.72794	328.9	6.0
53988.73584	330.3	5.8
53993.71885	306.6	7.7
54014.66291	-175.4	5.5
54016.65503	-236.1	5.4
54035.60988	-147.1	5.1
54039.58877	-29.0	5.2
54055.55127	302.5	5.6
54063.54556	327.1	5.7
54165.01752	-354.1	6.4
54167.00332	-362.1	6.4
54190.93933	182.1	6.4
54251.77452	-106.8	5.5
54323.81680	-86.4	5.5
54332.79368	173.3	7.9
54335.79347	228.2	6.0
54338.78881	275.7	6.3
54340.77677	301.3	6.1
54344.77039	324.4	6.3
54365.69757	22.9	6.3
54396.61972	-44.4	5.5
54400.59558	75.6	5.5

Table 44. HET Radial Velocities for HD 190228

JD-2400000	Velocity ( $\text{m s}^{-1}$ )	Uncertainty ( $\text{m s}^{-1}$ )
53581.89473	-75.5	8.2
53589.86259	-92.8	6.8
53605.81074	-83.7	9.0
53606.81111	-84.1	8.8
53607.80141	-84.9	8.4
53609.80786	-87.7	8.1
53628.75754	-85.0	7.8
53635.71968	-76.7	8.4
53653.67654	-81.1	7.5
53655.68368	-76.3	8.3
53686.58579	-61.1	9.0
53844.93852	-20.2	9.3
53867.88496	-34.8	9.3
53877.84874	-19.3	9.1
53883.82777	-12.2	8.2
53888.81145	-8.6	9.4
53897.79760	1.5	8.9
53935.90971	6.8	8.5
53956.84836	-9.1	7.5
53966.81728	-0.8	8.3
53976.79348	-2.1	8.4
53996.75947	5.3	9.0
53998.73191	7.8	9.4
53998.73697	-1.5	9.0
54008.70583	10.4	7.8
54013.70146	1.4	8.1
54019.66975	7.1	9.0
54032.62480	16.7	9.9
54217.92567	49.1	8.9
54265.79081	59.8	8.6
54284.96126	62.5	9.1
54326.62326	57.0	8.5
54328.62216	60.8	7.0
54331.61953	68.4	8.0
54336.59244	67.8	9.0
54344.79398	60.7	8.7
54352.77160	68.1	9.1
54368.71625	75.5	8.9
54370.72492	81.4	8.4
54377.68917	76.2	9.0
54401.62808	74.4	8.3
54428.57314	78.5	8.3

Table 45. 2.7m Radial Velocities for HD 190228

JD-2400000	Velocity (m s <sup>-1</sup> )	Uncertainty (m s <sup>-1</sup> )
53584.82785	-47.3	6.2
53585.80785	-27.8	8.9
53635.70876	-42.5	6.9
53636.74761	-41.8	5.5
53691.63145	-16.2	7.9
53862.94967	14.5	6.4
53927.85541	43.2	6.8
54403.65001	118.0	7.1